J. Nonlinear Sci. Vol. 10: pp. 223–274 (2000)
DOI: 10.1007/s003329910010

Journal of
Nonlinear
Science

The Geometry of the Phase Diffusion Equation

N. M. Ercolani,[1] R. Indik,[1] A. C. Newell,[1,2] and T. Passot[3]
[1] Department of Mathematics, University of Arizona, Tucson, AZ 85719, USA
[2] Mathematical Institute, University of Warwick, Coventry CV4 7AL, UK
[3] CNRS UMR 6529, Observatoire de la Côte d'Azur, 06304 Nice Cedex 4, France

Received on October 30, 1998; final revision received July 6, 1999
Communicated by Robert Kohn

Summary. The Cross-Newell phase diffusion equation, $\tau(|\vec{k}|)\Theta_T = -\nabla \cdot (B(|\vec{k}|) \cdot \vec{k}),\ \vec{k} = \nabla\Theta$, and its regularization describes natural patterns and defects far from onset in large aspect ratio systems with rotational symmetry. In this paper we construct explicit solutions of the unregularized equation and suggest candidates for its weak solutions. We confirm these ideas by examining a fourth-order regularized equation in the limit of infinite aspect ratio. The stationary solutions of this equation include the minimizers of a free energy, and we show these minimizers are remarkably well-approximated by a second-order "self-dual" equation.

Moreover, the self-dual solutions give upper bounds for the free energy which imply the existence of weak limits for the asymptotic minimizers. In certain cases, some recent results of Jin and Kohn [28] combined with these upper bounds enable us to demonstrate that the energy of the asymptotic minimizers converges to that of the self-dual solutions in a viscosity limit.

1. Introduction

The mathematical models discussed in this paper are motivated by physical systems, far from equilibrium, which spontaneously form patterns. When stressed beyond some threshold, the continuous translational symmetry of a spatially extended system breaks and a pattern forms; the continuous symmetry becomes a discrete symmetry. For example, in the formation of striped planar patterns in two dimensions, the continuous symmetry is locally preserved in one direction while in the perpendicular direction it reduces to a discrete periodic symmetry. Convection patterns in ordinary fluids and liquid crystals [11], [18], [29], [34], [45] and optical patterns in Raman and Maxwell-Bloch laser systems [27], [36] are just some of the striking examples of pattern formation.

Defects are also a universal feature of these systems. These are points and curves (points, curves, and surfaces in three dimensions) where the regularity of the pattern, seen as a macroscopic object, breaks down. Just as the planforms (stripes, squares, hexagons)

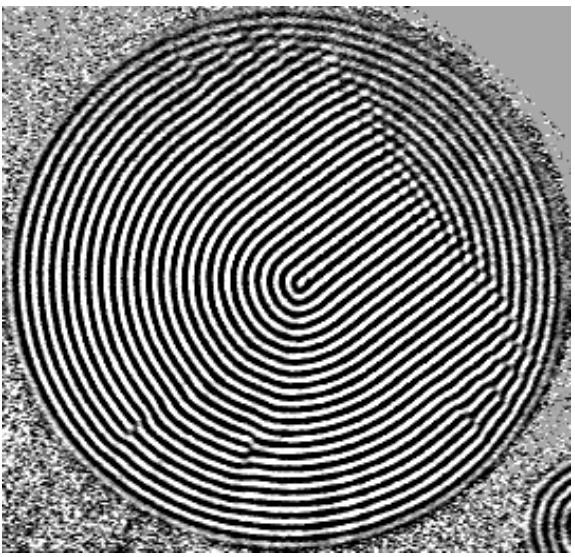

Fig. 1. Convection rolls from a Rayleigh-Bénard experiment [8].

observed in two-dimensional patterns are universal for a wide class of systems sharing certain symmetries, so too is the set of defects universal. A major goal of this work is to identify and classify the types of pattern defects that occur in systems with rotational symmetry.

Much of the intuition and terminology used to describe pattern formation has grown out of the vast physical literature concerning Rayleigh-Bénard convection [49], [12]. In a laboratory setting, convection is studied by trapping a fluid between two horizontal plates with a small separation between them and then heating the fluid from below. There is a parameter R, the Rayleigh number, which is proportional to the temperature difference between the bottom and top plates. For $R < R_c$, a critical value, heat is conducted but the fluid does not move. However, when R crosses this threshold, the fluid is set in motion and a pattern of "convection rolls" emerges.

The primary instability in convection was explained by Rayleigh using the Boussinesq approximation [15]. This analytical model consists of the Navier-Stokes equation to describe the fluid velocity coupled to a scalar diffusion equation which describes the evolution of the temperature. Near threshold, solutions of these equations predominantly have the form of almost straight parallel roll patterns. The behavior of these solutions can be well modeled by traditional amplitude equations [47], [56], [18], [45]. In this case, because both the amplitude and the phase are active order parameters when sufficiently close to threshold, these patterns display only restricted types of defects called dislocations and amplitude grain boundaries. In their vicinity, the amplitude of the velocity field envelope nearly vanishes.

Far from threshold, one discovers a much richer variety of defects [4], [53], [52]. For example, Figure 1 shows a result from a recent series of convection experiments [8] in

which high pressure CO_2-gas was used rather than more common fluids such as water and helium. This apparatus has the advantage that the height of the convection cell can be made very small so that a large aspect ratio (length to height ratio of the apparatus) can be obtained. The figure illustrates one of the types of defects that appear far from threshold and in which the amplitude of the field is not nearly vanishing. At the core of the figure there is a defect which is known as a *convex disclination*. (There are also dislocations in the outer regions of the figure.)

Mathematical models of pattern behavior far from threshold are equations derived for a phase order parameter which locally organizes the pattern. These equations are derived from solvability conditions associated with translational invariance. The purpose of this paper is to begin to explore such a model—the "Cross-Newell phase diffusion equation" (CN) [51]. First, we show through explicit analytical construction of approximate weak solutions to CN, that the level sets of these solutions and their singularities can provide good qualitative agreement between experimentally and numerically observed patterns and their defects. Second, we characterize the generic defects of solutions to CN so that they can be compared with observed defect types. Finally, we will consider a natural regularization of CN (RCN) which is variational. We show that the energy of its minimizers, appropriately scaled, tends asymptotically to the energy of our weak solutions as the regularization is removed.

From the mathematical point of view, CN is challenging. It formally supports singular and multivalued stationary solutions. One can try to select a single valued weak solution of this equation as a singular limit of solutions to the regularization, RCN. This is analogous to what one does in studying singular (zero viscosity) limits of Burgers' equation in order to describe shock formation. Consideration of the relation between limit solutions of RCN and those of CN provides a canonical model of a singular limit for an elliptic variational problem producing weak solutions with defects along one-dimensional curves. These problems are interesting because they are on the border of what can currently be understood analytically, as will be explained in Section 4. We remark that RCN has arisen independently in contexts other than pattern formation, such as thin film blisters [50], crumpled elastic sheets [54], [41], and liquid crystals [39].

The outline of this paper is as follows. In Section 2 we present background on the Cross-Newell equation and its regularization, including a derivation of the CN equation, a discussion of its physical interpretation, and a concise analysis of the type of the CN equation and how it can change. In particular, Section 2.3 unites and provides complete details of these latter results which we have cited elsewhere [51], [44], [9], including a description of the characteristics of the stationary Cross-Newell equation and their compatibility with standard descriptions of the linear stability of the microscopic equations (such as the Busse balloon). Section 2 continues with a discussion of singularities of CN and their topology. Finally the regularized equation (RCN) is introduced and shown to be variational.

In Section 3 we find exact solutions of the stationary CN equation via the Legendre transform leading to a hodograph equation. This produces a separable linear equation which we solve and analyze. The solutions constructed in this way are multivalued and their branch points represent caustic singularities. This application of the Legendre transform allows one to construct a complete solution of the CN equation in terms of multivalued analytic functions. To make contact with the original physical problem, we

discuss the jump conditions that a weak solution which patches together the different branches of a multivalued solution must satisfy. While we are not able to construct such general weak solutions that satisfy specified boundary conditions, we can produce solutions that satisfy the jump conditions (asymptotically) in the physically relevant case where the wavenumber is close to its preferred value on both sides of the shock.

In Sections 4 and 5 we turn our attention to the regularized Cross-Newell equation. The results of this section can be read independently of Section 3. In Section 4 the ansatz of self-dual reduction, an equipartition assumption, is used to reduce the fourth-order RCN equation to a second-order equation that we refer to as the self-dual equation. We show that a solution of the self-dual equation will be a solution of the RCN equation if the graph of the solution, viewed as a nonparametric surface, has zero Gaussian curvature. Numerical evidence [9] strongly suggests that the Gaussian curvature is zero almost everywhere. In an appropriate limit the self-dual equations can be transformed into a Helmholtz equation. The explicit solutions of this equation are analyzed in the vanishing viscosity limit. The resulting defects of these solutions are classified. Finally, in Section 5, we use the fact that stationary RCN is variational to analyze the minimizers of the associated free energy and their viscosity limits. In certain cases related to the self-dual solutions discussed in Section 4, we are able to describe the leading order asymptotic behavior of these minimizers. In particular upper bounds on the free energy are found. Thanks to some recent work of Jin and Kohn [28], in some of these cases we can also get good lower bounds on the free energy. In these same cases the upper and lower bounds can be evaluated on self-dual solutions and shown to be equal asymptotically.

2. Background

2.1. Formal Derivation of the Cross-Newell Equation

We believe that the regularized phase diffusion equation (RCN), which is the macroscopic equation to be discussed here, has validity in describing a wide variety of physical pattern-forming systems and in particular those which are close to gradient systems such as the case of high Prandtl number convection. However, to be explicit, we will restrict our consideration to the context of the Swift-Hohenberg (SH) equation,

$$w_t = -(1+\Delta)^2 w + Rw - w^3, \tag{1}$$

a well studied phenomenological model for Rayleigh-Bénard convection at high Prandtl number. The scalar independent variable w: $\mathbb{R}^2 \to \mathbb{R}$ represents the passively advected temperature scalar of the Boussinesq equations. Up to translation, the pattern is given by the level lines $w = c_0$ for a fixed value c_0.

Equation (1) is a gradient flow $w_t = -\frac{\delta \mathcal{E}}{\delta w}$ where

$$\mathcal{E} = \frac{1}{2}\int_\Omega \left(((1+\Delta)w)^2 - Rw^2 + \frac{1}{2}w^4 \right) dx\, dy, \tag{2}$$

and Ω is a region in the physical plane. Equation (1) admits a family of stationary "straight" roll solutions $w_0 = f(\theta)$ where f is an *even*, 2π-periodic function of θ [16]:

$$w_0 = a_1(k)\cos(\theta) + a_2(k)\cos(2\theta) + \cdots + a_n(k)\cos(n\theta) + \cdots, \tag{3}$$

with $\theta = \vec{k} \cdot \vec{x}$ and $k = |\vec{k}|$. Recursion formulae for the a_n are given in [16]; these also depend on R but this dependence is suppressed here. This family is parametrized by the wavevectors $\vec{k} \in \mathbb{R}^2$.

For equations such as (1), a general description of the stable stationary solutions beyond a fixed "planform" (straight rolls, squares, hexagons) does not yet exist. One can, however, appeal to an asymptotic method, modulation theory [59], to describe patterns that are locally of the form of stationary straight roll solutions but vary slowly over large distances. One thinks of the small parameter ϵ as being, in this context, the inverse of the aspect ratio mentioned above (the ratio of the plate separation to the diameter of the apparatus). When defects are present the appropriate definition of ϵ needs to be the inverse of the mean distance between defects. For the SH model this amounts to saying that there are many ($\mathcal{O}(\epsilon^{-1})$) rolls in the region Ω with sparse defects. One also wants these solutions to look locally like the straight roll solutions (3). So, formally, we seek solutions of the form $w = w^\epsilon(\Theta/\epsilon)$ whose argument depends only on the macroscopic or "slow scale" $(\vec{X}, T) = (\epsilon\vec{x}, \epsilon^2 t)$; i.e., $\Theta = \Theta(\vec{X}, T)$. The microscopic or "fast" scale of the solution is expressed through the periodic function w^ϵ being scaled by $1/\epsilon$. The organizing idea here is that this w should, locally in space (i.e., in a region the diameter of a few roll widths) and time, "look like" a stationary solution (3), but only approximately. The modulation is represented as a slow variation of wavevector $\vec{k}$ which parameterizes the family (3). Thus, one thinks of $w^\epsilon(\Theta/\epsilon)$ as having the form of (3) but with Θ and the Fourier coefficients $a_n(k)$ modulated (through the modulation of $\vec{k}$). While on the local scale $\vec{k}$ is constant, on the macroscopic scale it varies: $\vec{k} = \vec{k}(\vec{X}, T)$.

To make these ideas into a formally self-consistent perturbation scheme, one defines the wavevector by

$$\vec{k} = \nabla_{\vec{X}}\Theta.$$

Thus instead of defining θ in terms of $\vec{k}$ (as $\theta = \vec{k} \cdot \vec{X}$), we define $\vec{k}$ in terms of the slowly varying Θ. The fast dependence in w^ϵ is then represented by those expressions which depend on the fast phase $\theta = \epsilon^{-1}\Theta$. We also mention that the choice of a parabolic scaling for time is essentially dictated by the fact that the background solutions (3) are stationary. If the background solutions were traveling waves, the analysis we are about to describe would require two slow time scales, $T_1 = \epsilon t$; $T_2 = \epsilon^2 t$, where T_1 is related to the modulation of the background frequency [33], [35], [37].

Next, one wants to evaluate the SH equation (1) on the modulated form of (3) which we represent as

$$w^\epsilon(\vec{X}, T) = w_0 + \epsilon w_1 + \epsilon^2 w_2 + \cdots.$$

Based on this ansatz and formal application of the chain rule, one can represent the space and time derivatives of w^ϵ as

$$\begin{aligned} \partial_t &= \epsilon^2 \Theta_T \partial_\Theta + \epsilon^2 \partial_T \\ &= \epsilon \Theta_T \partial_\theta + \epsilon^2 \partial_T, \\ \nabla_{\vec{x}} &= \epsilon \nabla_{\vec{X}} \Theta \partial_\Theta + \epsilon \nabla_{\vec{X}} \\ &= \vec{k} \partial_\theta + \epsilon \nabla_{\vec{X}}. \end{aligned}$$

Using these representations one easily finds that the fourth-order operator in SH expands as

$$(1+\Delta)^2 = \mathcal{L}_0 + \epsilon\mathcal{L}_1\partial_\theta + \epsilon^2\mathcal{L}_2 + \epsilon^3\mathcal{L}_3\partial_\theta + \epsilon^4\mathcal{L}_4,$$

where $\mathcal{L}_0 = (1+k^2\partial_\theta^2)^2$, $\mathcal{L}_1 = (1+k^2\partial_\theta^2)D_1 + D_1(1+k^2\partial_\theta^2)$ with $D_1 = 2\vec{k}\cdot\nabla + (\nabla\cdot\vec{k})$, and so on.

Evaluating SH on w^ϵ, one finds at leading order that

$$(\mathcal{L}_0 - R)w_0 + w_0^3 = 0.$$

This is precisely the equation satisfied by the straight roll solutions of [16]. If one takes w_0 here to be one of the solutions (3), then this is consistent with the ansatz that w^ϵ should locally "look like" a straight roll solution. However, although w_0 here has the form of (3), it should not be thought of as one of these solutions since it will depend on the slow variable $\vec{X}$ through k in the Fourier coefficients. This dependence can be accessed through the first correction which satisfies

$$(\mathcal{L}_0 - R + 3w_0^2)w_1 = -\partial_\theta w_0\Theta_T - \mathcal{L}_1(\partial_\theta w_0).$$

The null space of $\mathcal{L}_0 - R + 3w_0^2$ acting on 2π-periodic functions of θ contains the marginal mode $\partial_\theta w_0$. Thus there is a formal solvability condition for w^ϵ to maintain the form of a 2π-periodic function of θ:

$$\langle\partial_\theta w_0|\partial_\theta w_0\rangle\Theta_T + \langle\partial_\theta w_0|\mathcal{L}_1\partial_\theta w_0\rangle = 0,$$

where $\langle a|b\rangle = 1/2\pi\int_0^{2\pi} ab\,d\theta$.

Setting $\vec{k} = k\hat{k}$, where $\hat{k}$ denotes the unit vector in the direction $\vec{k}$, expanding and performing the averages in the above solvability condition, one arrives at the Cross-Newell phase diffusion equation which has the form

$$\Theta_T - kD_\perp(k)\nabla\cdot\hat{k} - D_{||}(k)\hat{k}\cdot\nabla k = 0. \tag{4}$$

One refers to $D_\perp(k)$ and $D_{||}(k)$ as the (resp.) perpendicular and parallel diffusion coefficients of the system. These will be explicitly given in Section 2.2. For full details of the above modulational analysis see [51].

2.2. Physical Interpretation of the Cross-Newell Equation

The representation (4) is what gave rise to the terminology *phase diffusion*. In the vicinity of straight, parallel, equally spaced rolls with common wavevector $\vec{k}_0$, equation (4) is often regarded as an equation with fixed diffusion coefficients. Since $\nabla\cdot\hat{k}$ is the curvature of a roll, the perpendicular diffusion coefficient $D_\perp(k_0)$ measures the response of the system to bending of the rolls. Similarly, $\hat{k}\cdot\nabla k$ describes the local change in spacing of roll crests, and the parallel diffusion coefficient $D_{||}(k_0)$ measures the response of the system to the compression or expansion of rolls in a direction perpendicular to their axes. The physical meaning of *phase-diffusion* is that any deviation of the rolls from being straight and parallel, with spacing of 2π, should "diffuse" away, restoring the rolls to this

preferred state. Recent work [55], [21], [58] demonstrates that for the SH equation, *near threshold*, the marginally stable stationary straight roll solutions of [16] are nonlinearly stable. This provides strong support for the validity of the modulational ansatz. Of course, as in geometric optics, these modulation equations have formal validity only so long as the variation of the rolls is sufficiently gradual.

A diffusion equation having the form of a linearization of (4),

$$\Theta_T - D_\perp(k_0)\partial_X^2\Theta - D_{||}(k_0)\partial_Y^2\Theta = 0,$$

was first written down by Manneville and Pomeau [42], who derived it from the Newell-Whitehead-Segel equation [47], [56] as the corresponding phase equation. However, unlike [19], their derivation was formally valid only near threshold (in the context of SH this would mean for R small). What characterizes CN is that the small parameter corresponds to the inverse aspect ratio of the system and the derivation is carried out by modulating straight roll solutions.

The derivation of the CN equation for a wide variety of stationary pattern-forming equations was worked out, for example, in [19], [46], [51]. In all these cases, the modulation equation can be rewritten in divergence form as

$$\tau(k^2)\Theta_T = -\nabla_{\vec{X}} \cdot (\vec{k}B(k^2)), \tag{5}$$

where the diffusion coefficients are recovered as $kD_\perp = -kB/\tau$ and $D_{||} = -(kB)_k/\tau$. For SH, $\tau(k^2) = \langle(\frac{\partial w_0}{\partial\theta})^2\rangle$ and $B(k^2) = \frac{1}{2}\frac{d}{dk^2}\langle w_0^4\rangle$, where $\langle\cdot\rangle = \frac{1}{2\pi}\int\cdot d\theta$ is the phase average with respect to θ. The *stationary* form of (5) is given by

$$\begin{aligned} \nabla_{\vec{X}} \cdot (\vec{k}B(k^2)) &= 0, \\ \nabla_{\vec{X}} \times \vec{k} &= 0, \end{aligned} \tag{6}$$

where $\vec{k} \stackrel{\text{def}}{=} \nabla_{\vec{X}}\Theta$. These equations are the variational equations $\tau(k^2)\Theta_T = -\delta\mathcal{I}/\delta\Theta$ for the free energy

$$\mathcal{I} = \frac{1}{2}\int_\Omega G^2(k^2)\, dX\, dY, \tag{7}$$

where $G^2(k^2) = -\int_{k_B^2}^{k^2} B(s)\, ds$, where k_B is chosen so that the minimum of $G^2(k^2)$ is zero.

For the Swift-Hohenberg equation $G^2(k^2) = -\frac{1}{2}\langle w_0^4\rangle$ is transcendental. For concreteness here, we will approximate w_0 by the first term in its Fourier expansion (which is in fact valid close to threshold). In this truncation B and τ can be approximated by polynomials as

$$\begin{aligned} kB(k^2) &\approx 2k(1-k^2)(R-(1-k^2)^2), \\ \tau(k^2) &\approx (R-(1-k^2)^2). \end{aligned} \tag{8}$$

The cubic-like profile of kB, common to a large class of microscopic systems, is displayed in Figure 2b. The energy density for this approximation,

$$G^2(k^2) = \frac{1}{4}(R^2 - (R-(1-k^2)^2)^2), \tag{9}$$

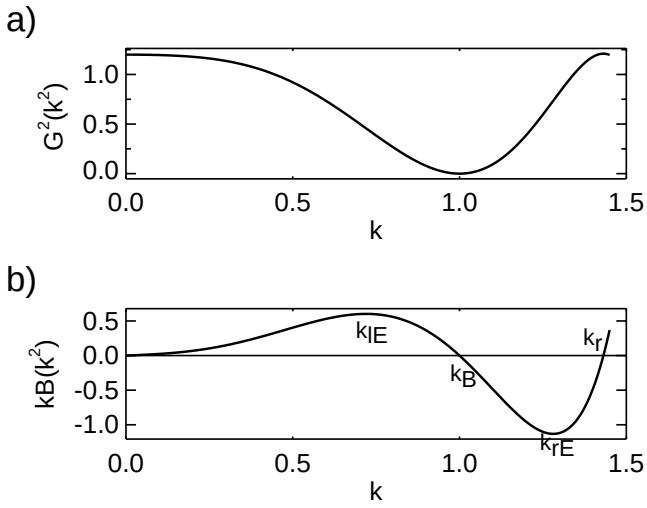

Fig. 2. (a) CN energy density as a function of k. (b) Corresponding $(kB(k^2))$.

is graphed in Fig. 2a. Whenever one of the diffusion coefficients crosses zero, the system (6) changes type. Figure 2b indicates where these crossings occur. In particular the range of wavenumbers between k_B and k_{rE} constitutes the range of linearly stable wavenumbers in the vicinity of the straight roll solutions. In this range, known as the Busse balloon [11], (4) is a quasilinear diffusion equation for Θ whose spatial part (the RHS of (4)) is a positive elliptic operator.

2.3. Nonlinear Structure of the Cross-Newell Equation

We explore further the mathematical structure of the stationary phase diffusion equation (6). As we just mentioned, this is a quasilinear equation of mixed type. In order to identify the different elliptic and hyperbolic regimes of this equation as well as to describe its multivalued analytic solutions, it will be useful to introduce the quadratic form, with entries depending on (f, g),

$$\mathbf{Q} \stackrel{\text{def}}{=} B\mathbf{1} + 2B'\vec{k} \cdot {}^{\mathbf{t}}\vec{k},$$

(where $' = \frac{d}{dk^2}$) and its adjugate form

$$\mathbf{Q}^{adj} = B\mathbf{1} + 2B'\vec{n} \cdot {}^{\mathbf{t}}\vec{n},$$

where $\vec{n} = J\vec{k}$ and $J = \left(\begin{smallmatrix} 0 & -1 \\ 1 & 0 \end{smallmatrix}\right)$. The adjugate of a matrix M is implicitly defined by $M \cdot M^{adj} = det(M)\mathbf{1}$. The stationary equation may now be expressed as the vanishing trace of a product of quadratic forms,

$$\begin{aligned} \nabla_{\vec{X}} \cdot (\vec{k}B) &= \mathrm{Tr}\{\mathbf{Q} \cdot D^2_{\vec{X}}\Theta\} \\ &= (B + 2B'f^2)\Theta_{XX} + 4B'fg\Theta_{XY} + (B + 2B'g^2)\Theta_{YY} = 0, \quad (10) \end{aligned}$$

with $D^2_{\vec{X}}\Theta$ construed as the Hessian of Θ. The characteristic ODE is then given by

$$ {}^t\mathbf{d}\vec{X}\mathbf{Q}^{adj}\mathbf{d}\vec{X} = (B + 2B'f^2)dY^2 - 4B'fgdXdY + (B + 2B'g^2)dX^2 = 0. \tag{11} $$

The eigenvectors of $\mathbf{Q}$ are $\vec{k}$ and $\vec{n}$. One easily sees from its definition that

$$ \mathbf{Q}\vec{k} = (kB)_k\vec{k}, \tag{12} $$

$$ \mathbf{Q}\vec{n} = B\vec{n}. \tag{13} $$

Note that the eigenvalues are proportional to the parallel and perpendicular diffusion coefficients appearing in (4). Since $\mathbf{Q}$ and its adjugate are similar,

$$ \mathbf{Q} = {}^t J\mathbf{Q}^{adj}J, \tag{14} $$

$\mathbf{Q}^{adj}$ has the same eigenvalues as $\mathbf{Q}$ with the corresponding eigenvectors rotated 90°. In particular, the stationary phase diffusion equation is elliptic when both diffusion coefficients have the same sign and hyperbolic when the signs are opposite. These eigenvalue signatures partition the wavenumber ranges as follows (see Figure 2b):

$$ \begin{aligned} &k_{lE} < k < k_B \Rightarrow B > 0, (kB)_k < 0 \qquad \text{(hyperbolic)}, \\ &k_B < k < k_{rE} \Rightarrow B < 0, (kB)_k < 0 \qquad \text{(elliptic)}, \\ &k_{rE} < k < k_r \Rightarrow B < 0, (kB)_k > 0 \qquad \text{(hyperbolic)}. \end{aligned} \tag{15} $$

The *characteristic speeds* $\lambda_\pm$ (we use this terminology even when our equation is elliptic) can be determined from (11) by the quadratic formula:

$$ \begin{aligned} \lambda_\pm &= 2B'fg \pm \sqrt{4(B'fg)^2 - (B + 2B'f^2)(B + 2B'g^2)} \\ &= 2B'fg \pm \sqrt{-B(kB)_k}. \end{aligned} \tag{16} $$

Comparing this with (15) one sees that the speeds become equal only at places where the equation changes type between elliptic and hyperbolic, i.e., where one of the eigenvalues of $\mathbf{Q}$ becomes zero.

The elliptic interval between k_B and k_{rE} is frequently referred to as the *Busse balloon* [11]. One understands the significance of the Busse balloon by considering the second derivative of the free energy (7) which can be represented in terms of the quadratic form $\mathbf{Q}$. On the family of perturbations $\Theta^{(\delta)} = \Theta^{(0)} + \delta\Theta^{(1)}$ with $0 \le |\delta| \le 1$, the free energy can be expanded by Taylor's theorem as

$$ \begin{aligned} \mathcal{I}^\delta &= \mathcal{I}^0 - \delta\int\int_U dX\,dY\vec{k}^{(0)}B(k^{(0)2})\cdot\vec{k}^{(1)} \\ &\quad - \frac{1}{2}\int_0^\delta(\delta - s)\left\{\int\int_U dX\,dY({}^t\vec{k}^{(1)})\mathbf{Q}^{(s)}(\vec{k}^{(1)})\right\}ds, \end{aligned} \tag{17} $$

where $\mathbf{Q}^{(s)}$ is $\mathbf{Q}$ evaluated on $\Theta^{(s)}$.

If one takes $\Theta^{(0)}$ to be a solution of the stationary equation, then the order δ term vanishes entirely. Moreover, if $-\mathbf{Q}^{(0)}$ is positive definite in a neighborhood $\Theta^{(0)}$, then for $\Theta^{(1)}$ sufficiently small so is $-\mathbf{Q}^{(s)}$ for $0 \le s \le \delta$. It follows that in this case $\mathcal{I}^{(0)} < \mathcal{I}^{(\delta)}$,

and therefore any solution of the stationary phase diffusion equation whose wavevectors $\vec{k}$ always lie in the Busse balloon is a local minimum of the energy. On this neighborhood $\mathcal{I}$ would be convex.

On the other hand if $\Theta^{(0)}$ is a solution for which $\mathbf{Q}^{(0)}$ has a negative eigenvalue at some point, then the energy can be lowered by an arbitrarily small perturbation. To see this observe from (12) and (15) that in the interval (k_{lE}, k_B) (resp. (k_{rE}, k_r)), $\vec{n}$ (resp. $\vec{k}$), is the direction of maximal decrease of $\mathcal{I}$ at $\Theta^{(0)}$. Taking $\Theta^{(1)} = \Psi^{(0)}$(resp. $\Theta^{(0)}$) lowers the energy $\mathcal{I}^{(\delta)}$ below $\mathcal{I}^{(0)}$. Therefore, in the functional vicinity of any solution having $k < 1$ in some region of the $\vec{X}$-plane, the energy is nonconvex. For the solutions that we shall explicitly construct in Section 3.2 this will be the case. In the time-dependent setting (5), this nonconvexity implies that the stationary solution is unstable. This instability, known in the literature as the zig-zag instability, is one of the problems which force us to consider a regularization of the Cross-Newell equation.

Equation (10) has a form that appears in many other mathematical contexts. One such is the equation for nonparametric minimal surfaces in $\mathbb{R}^3$. These are locally area-minimizing surfaces among surfaces presented as a graph $Z = h(X, Y)$. The analogue of the free energy in this problem is the area functional of the surface. Here $B = (1 + h_X^2 + h_Y^2)^{-1/2}$ and the energy integrand is $\int kB(k^2)\,dk = (1 + h_X^2 + h_Y^2)^{1/2}$. The analogue of the rolls are the level sets of the minimal surface. There is a vast literature on this problem [48]. We will exploit this geometric analogy in our analysis of defects in Section 3. Another example is the equations for 2D stationary, ideal, isentropic gas dynamics [17]. Here $\vec{k}$ is the fluid velocity and $B(k^2)$ is the density. The energy integrand is this fluid density, and the gas dynamics equations are the variational equations for this energy. A particularly challenging aspect of these equations is to describe (weak) solutions in the transonic regime where the equation changes type from hyperbolic to elliptic. The phase diffusion equation is more difficult than these classical examples because its $B(k^2)$ is not monotone.

2.4. Singularities

In the immediate vicinity of a defect where one can see that the wavevector changes rapidly, the modulational ansatz is no longer even formally valid, and in fact the stationary equation (6)—when solved by the method of characteristics—develops multivalued solutions, as will be described in Section 3. Nevertheless, we will see that the unregularized equation supports explicit solutions that give an excellent representation of some of the most frequently observed isolated stationary defects. Two types of defects arise in this setting. One type is related to *caustics*, which are envelopes of characteristics of the system (6)—i.e., places where characteristics begin to collide. Their presence indicates that the solution has become multivalued and therefore can no longer be classical. Caustics correspond to curves in the (X, Y)-plane where the solution changes from one branch to another. The other type of defect is a *point defect*. Whereas caustics represent a geometric obstruction to the existence of a global classical vector field solution of (6), a point defect is a topological obstruction to the existence of global *gradient* vector field solutions, although local gradient solutions will exist everywhere away from point defects.

2.4.1. Twist and the Topology of Point Defects. At the most fundamental level, our experience of roll patterns is as a family of stripes. In the case of Swift-Hohenberg, for example, these stripes may locally look like the level curves of a function such as $\cos(\vec{k}_0 \cdot \vec{X})$, at least away from defects. The phase Θ itself need not be well defined (for instance, $\Theta \to -\Theta$ leaves the pattern unaltered). The existence of these ambiguities is intimately related to the types of defects that can occur. The second equation in (6), $\nabla_{\vec{X}} \times \vec{k} = 0$, allows us to conclude the *local* existence of a potential, Θ, for $\vec{k}$; i.e., $\nabla\Theta = \vec{k} = (f, g)$. Defects in the pattern can be obstructions to the extension of the local potentials to a single global one. This obstruction is topological. To gain some insight into the purely topological aspects of defects in our problem, we consider equation (6) with $B = 1$. In this case the equations are linear (in fact, they are equivalent to Laplace's equation). Figure 3 shows some examples of canonical patterns with defects. This does capture the topological character of defects; what is different for the case $B = 1$ is that the associated energy density has no minima. Hence, there is no mechanism for selecting a preferred wavenumber k.

In Figure 3a we have tried to consistently plot a vectorfield along a box surrounding the defect. We see that this attempt must fail; the vector returns to its starting point with its orientation reversed. The angle through which the vector rotates in traversing a counterclockwise circuit, divided by π, is called the *twist* [43], [31] of the defect. Thus Figures 3a, 3b have twist $-1, +1$, respectively. Figures 3c, 3d which have twist ∓ 2 do in fact have global potentials, although the potential for Figure 3d is undefined at the defect. In these patterns the local wavevector $\vec{k}$ is defined only up to a sign $\pm\vec{k}$. To define a global field with odd twist it is often convenient to consider the slightly weaker notion of a *director* field [18], which does not distinguish between $+\vec{k}$ and $-\vec{k}$.

Finding solutions of equation (10) with nontrivial twist is a challenging problem. In Section 3 we show how to construct some solutions of this type on the complement of a small neighborhood of the defects. In particular we construct such solutions having single point defects of twist -1 or $+1$.

2.4.2. Caustics. Singularities which we refer to as *caustics* are probably best exemplified in the context of geometric optics where they arise as envelopes of rays. To be precise let us consider the example of an elliptical domain Ω with rays emanating normally to the boundary, $\partial\Omega$, of this ellipse and directed towards its interior as indicated in Figure 4a. To be specific, in what follows $\vec{X}_0(s)$ is the counterclockwise unit-speed arclength parametrization of $\partial\Omega$ and $\vec{N}(s) = J\vec{X}_0(s)$ is the inward pointing unit normal.

In this example, the analogue of a multivalued solution of the CN equation that we will construct is the ray surface, which is defined to be

$$\left\{(\vec{X}, Z)\colon\ \vec{X} = \vec{X}_0(s) + t\vec{N}(s) \quad \text{and} \quad Z = t \text{ for } (s, t) \in (0, L) \times \mathbb{R}\right\},$$

where L is the length of the ellipse. This surface is ruled by the rays that are the lines in the ray surface gotten by fixing $s = s_0$. The level curves of this multivalued ray surface are gotten by taking a horizontal slice at $t = t_0$; i.e., these are the loci of *locally* equidistant points to $\partial\Omega$. A few of these level curves are shown in Figure 4b which shows the development of caustic singularities when t gets large enough.

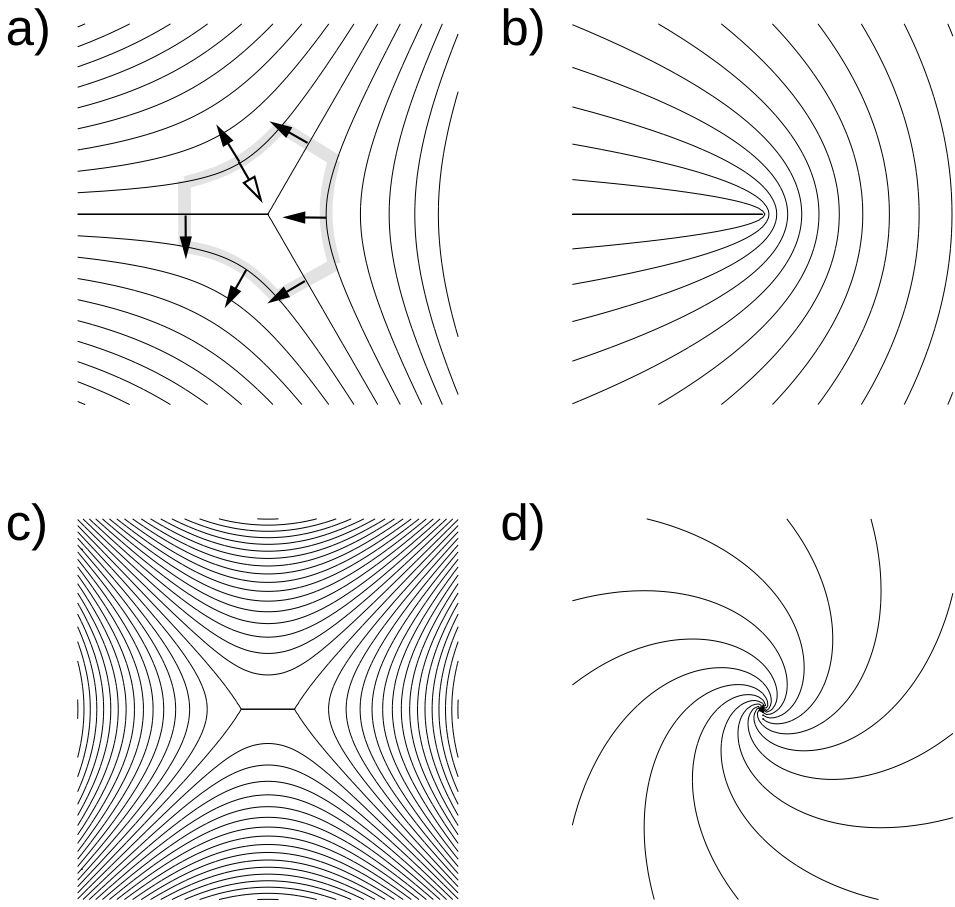

Fig. 3. Trajectories of harmonic ($B = 1$) director fields with defects (a) of twist -1; (b) of twist $+1$; (c) two of twist -1; (d) of twist $+2$.

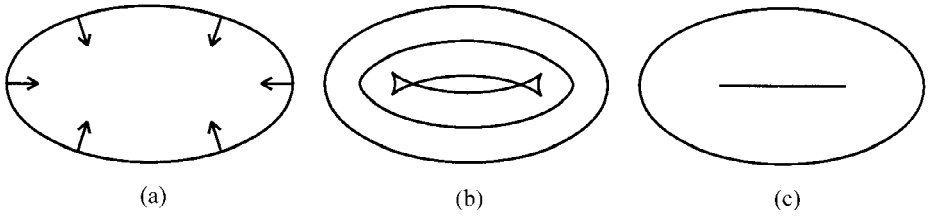

Fig. 4. Aspects of a ray surface from an elliptical boundary: (a) rays, (b) level curves, (c) defect locus.

On the other hand one can introduce a single-valued truncation of the ray surface which is simply the function $d(\vec{X})$ on Ω defined to be the distance from $\vec{x}$ to the boundary of the ellipse; i.e., $d(\vec{x}) = \text{distance}\,(\vec{X}, \partial\Omega)$. The graph of this function is smooth away from places $\vec{X}$ for which there is more than one point on $\partial\Omega$ having the same distance to $\vec{X}$. Such nonsmooth points are part of the *defect locus* of this surface shown in Figure 4c as the horizontal segment on the X axis whose endpoints are located at the two curvature centers of the ellipse.

Above this locus, two branches of the ray surface intersect. This intersection occurs before the corresponding rays have a chance to reach a caustic (excepting the curvature centers at the endpoints of the defect, which are incipient caustics).

Multivalued surfaces having caustic singularities of this form arise naturally as Legendre transforms of nonconvex functions. If $\hat{\Theta}(\vec{k})$ is such a function, then its Legendre transform $\Theta(\vec{X})$ is implicitly defined by the relation

$$\Theta(\vec{X}) + \hat{\Theta}(\vec{k}) = \vec{k} \cdot \vec{X}.$$

As will be explained in Section 3.1, when $\Theta(\vec{X})$ is a solution of the stationary CN equation, $\hat{\Theta}(\vec{k})$ solves a hodograph equation in which the roles of the independent and dependent variables are interchanged. The advantage of this hodograph equation is that it is linear and so it is a more tractable equation to solve and analyze. The Legendre transform is a differentiable map from $\vec{k}$-space and $\vec{X}$-space. Caustics are analytically described as the image in $\vec{X}$-space of the locus where the Jacobian ($J = X_f Y_g - X_g Y_f$) of the Legendre map vanishes.

Figure 5 illustrates the generic types of caustic singularities that arise in Legendre transforms of solutions to the hodograph equation associated to the stationary CN equation. The caustics are the bold dark lines corresponding to places where $J = 0$. Smooth points along these curves are referred to as *folds*. Cuspidal points such as those seen in part (a) of this figure are called *cusps*. Places where two branches cross, as in part (c) are called *umbilics*. Folds and cusps are generic singularities for general Legendre transformations as was originally shown by Whitney [60]. Umbilics only become generic when the additional constraint is imposed that $\Theta(\vec{X})$ should solve the stationary CN equation. The proof that, with this constraint, the above singularities are the only generic singularities will be described in [22], which applies results from [13].

One would like to pass from multivalued solutions of the CN solution to single-valued solutions with defects, analogous to what was done in the geometric optics example. However, unlike this example, a solution of the CN equation—or of the associated hodograph equation—does not have a natural notion of distance associated with it. Thus there is no obvious mechanism for selecting where the multivalued solution can be cut off, i.e., where the defect should be placed. In [22] we explore some examples in which a metric *can* be associated with a solution of the hodograph equation which may then be used to truncate the multivalued Legendre transform of this solution and so get an approximate solution of the CN equation with defects. Alternatively one can try to realize a single-valued weak solution of CN equation, as a singular limit of solutions to a regularization of this equation as one does in taking the zero-viscosity limit of the Burgers equation. This is what is done in Sections 4 and 5 of this paper. The next section reviews the background for this approach.

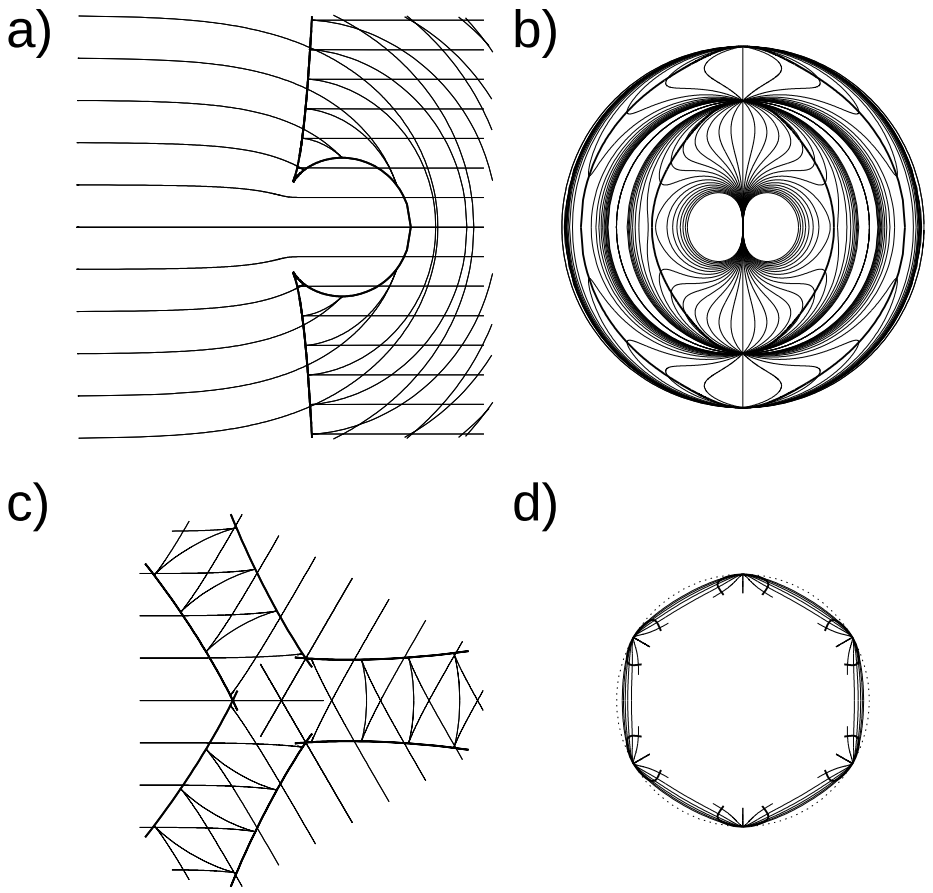

Fig. 5. Rolls in the physical plane (a), (c) and hodograph plane (b), (d). The bold dark lines in (a), (c) show the locus of $J = 0$. Note that in (a), (c) the cusps of the rolls lie on this locus.

2.5. The Regularized Cross-Newell Equation

To construct physically reasonable solutions, one needs to introduce a regularization of eqs. (5) and (6). This regularization comes in at order ϵ^3 since order ϵ^2 terms do not contribute to the phase equation. Among all terms at third order we only keep those which are dominant with respect to the small parameter $1 - k^2$. The same will be true in Section 4 for $B(k^2)$, which we shall approximate by $1 - k^2$. The resulting equation [19],

$$\tau(k)\Theta_T + \nabla \cdot \vec{k} B(k) + \eta\epsilon^2 \nabla^4 \Theta = 0, \tag{18}$$

and its small ϵ limit will be discussed in later chapters of this paper. Here, $\eta = |B_k(k_B)|/4k_B$. In the remainder of this paper we will, for convenience of notation, assume that $\eta = 1$. Near threshold Kuramoto added a similar fourth-order term to regularize an antidiffusive 1D phase equation which has become known as the Kuramoto-Sivashinsky equation. It is also interesting that a stationary version of (18) has recently been put

Fig. 6. A quasi-stationary solution of the Swift-Hohenberg equation at $R = 0.5$.

forward as a model for the formation of defects in the blistering of thin films [50], [28].

Figure 6 exhibits the rolls, i.e., level curves, of a stationary solution of SH. The equation is solved in a disk with $w = 0$ and $\partial w/\partial n = 0$ on the boundary and with initial data having symmetry under 120° rotation. This figure, which exhibits a concave disclination at the origin, is a snapshot taken when the solution has become effectively stationary.

One can see that these are far from straight roll solutions. The curvature in these rolls is due to the influence of boundary conditions and the fact that as R is raised above the critical threshold, $R_c = 0$, roll "patches" arising at different locations have uncorrelated orientations. The pattern is a mosaic of patches with different roll orientations, connected at grain boundaries (which are the rays at angles $\pi/3$, π, $5\pi/3$) that meet at the origin in a point defect.

Figure 7 shows a numerical solution of the *stationary* RCN equation (18) on a double cover of the disk. Notice that, away from a thin layer along the boundary, the agreement between Figures 6 and 7 is quite striking.

Figure 8 is another numerical solution of the stationary regularized phase diffusion equation also calculated on a double cover of the disk. The similarity of the structure of this numerically generated solution with that of the experimental pictures shown in Figure 1 provides some justification for the exploration of the Cross-Newell model.

The stationary RCN equation (18) is variational with free energy $\frac{\epsilon}{2}\mathcal{E}^\epsilon(\Theta)$,

$$\mathcal{E}^\epsilon(\Theta) = \int_\Omega \epsilon(\Delta\Theta)^2 \, d\vec{X} + 1/\epsilon \int_\Omega G^2(k) \, d\vec{X},$$

where $G^2 = -\int_{k_B^2}^{k^2} B \, dk^2$ and where Ω will generally be taken to be a simply connected domain in the plane. In general we will consider this energy functional on a class of functions with (possibly ϵ-dependent) Dirichlet boundary conditions.

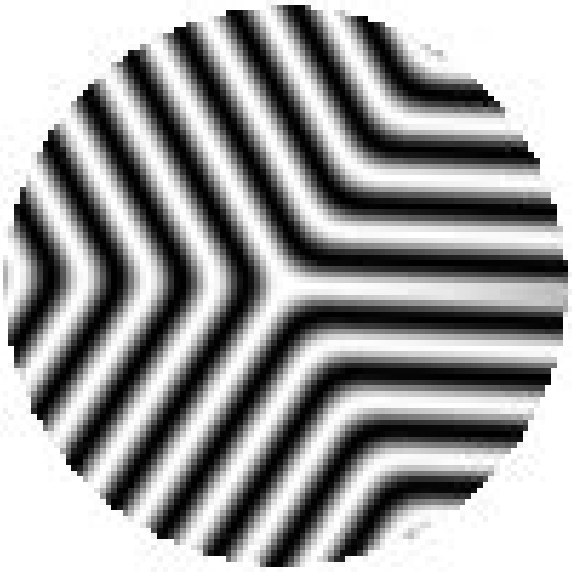

Fig. 7. A concave disclination of the regularized Cross-Newell equation.

As will be described in Section 4.1 we have found that functions in the above class which equipartition this free energy solve the variational equations of this energy away from places where the Gaussian curvature of the graph of Θ is nonzero. The support of this curvature concentrates on sets of vanishingly small measure as ϵ tends to zero. The energy is equipartitioned if Θ^ϵ solves

$$\epsilon \nabla^2 \Theta^\epsilon = \mp G.$$

We refer to solutions of either of these equations as *self-dual* solutions. Such solutions, used as test functions, are the key ingredient in estimating minimizers of the free energy $\mathcal{E}^\epsilon$, which is the subject of Section 5.

3. Exact Solutions of the Stationary Phase Diffusion Equation

This section presents detailed descriptions of solutions of the stationary phase diffusion equation. It is possible to construct all multivalued solutions of (6) whose expansion as a second-order scalar equation is given in equation (10), which we reproduce here for the reader's convenience:

$$\nabla_{\vec{X}} \cdot (\vec{k} B) = \mathrm{Tr}\{\mathbf{Q} \cdot D^2_{\vec{X}} \Theta\} = (B + 2B' f^2)\Theta_{XX} + 4B' fg \Theta_{XY} + (B + 2B' g^2)\Theta_{YY} = 0.$$

This section will describe and illustrate this construction. Our method uses the *Legen-*

Fig. 8. A convex disclination of the regularized Cross-Newell equation.

dre transform which interchanges the dependent variables $\vec{k} = (f, g)$ and the independent variables $\vec{X} = (X, Y)$ in (10). The induced equation for the inverted functions, $\vec{X}(\vec{k})$, is a linear partial differential equation called the *hodograph* equation, which turns out to be separable in polar coordinates ($f = k\cos\phi,\ g = k\sin\phi$).

3.1. Legendre Transform

The Legendre transform [17] provides an effective means for interchanging the roles of the dependent and independent variables of the phase diffusion equation, which will in fact linearize this equation. In this application it is often referred to as the hodograph transform. It also serves to describe the multivalued character of the analytic solutions to the phase diffusion equation. The Legendre transform $\hat{\Theta}$ of the phase Θ can be implicitly defined by

$$\Theta(\vec{X}) + \hat{\Theta}(\vec{k}) = \vec{k} \cdot \vec{X}. \tag{19}$$

Differentiating this relation,

$$\nabla_{\vec{X}}\Theta = \vec{k}, \qquad \nabla_{\vec{k}}\hat{\Theta} = \vec{X},$$
$$D^2_{\vec{X}}\Theta = \frac{\partial \vec{k}}{\partial \vec{X}}, \qquad D^2_{\vec{k}}\hat{\Theta} = \frac{\partial \vec{X}}{\partial \vec{k}},$$

one arrives at a relation between second derivatives

$$\begin{pmatrix} \Theta_{XX} & \Theta_{XY} \\ \Theta_{XY} & \Theta_{YY} \end{pmatrix} = J^{-1} \begin{pmatrix} \hat{\Theta}_{gg} & -\hat{\Theta}_{fg} \\ -\hat{\Theta}_{fg} & \hat{\Theta}_{ff} \end{pmatrix},$$

$$J \stackrel{\text{def}}{=} \left| \frac{\partial \vec{X}}{\partial \vec{k}} \right|, \tag{20}$$

from which the hodograph equation is immediate

$$tr\{\mathbf{Q}^{adj} \cdot D_{\vec{k}}^2 \hat{\Theta}\} = (B + 2B' f^2)\hat{\Theta}_{gg} - 4B' fg\hat{\Theta}_{fg} + (B + 2B'g^2)\hat{\Theta}_{ff} = 0.$$

This equation is manifestly linear. The characteristic ODE for the hodograph is

$${}^{\mathbf{t}}\mathbf{d}\vec{k}\mathbf{Q}\mathbf{d}\vec{k} = (B + 2B' f^2)df^2 + 4B' fgdfdg + (B + 2B'g^2)dg^2 = 0. \tag{21}$$

It follows from this and equation (14) that the stationary phase diffusion equation and its hodograph are both elliptic (respectively hyperbolic) iff $\mathbf{Q}^{adj}$, or equivalently $\mathbf{Q}$, is definite (respectively indefinite).

When the stationary phase diffusion equation is elliptic, one can show by an application of Holmgren's Theorem [24] that, with the possible exception of isolated point defects, the hodograph map $\vec{X}(\vec{k})$ is locally 1:1. In particular, J cannot vanish along a curve in elliptic regions without vanishing identically.

In nonelliptic regions J may vanish along curves. Then the hodograph map $\vec{X}(\vec{k})$ has folds and more complicated caustics. A consequence of this folding is that the analytic solutions of (6) are multivalued. Figure 5 illustrates the loci where $J = 0$ in the $\vec{k}$ plane and the corresponding caustics in $\vec{X}$. One can notice in this figure that the caustics are the envelope of places where rolls develop cusps and become multivalued.

Since $\mathbf{Q}^{adj}$ is definite in the elliptic region of (15), the ODE (11) has no nontrivial real solutions. On the other hand, in hyperbolic regions where $\mathbf{Q}^{adj}$ is indefinite, there are two families of characteristics solving (11) which give local coordinates on these regions.

3.2. Fundamental Hodograph Modes

Changing to polar coordinates,

$$(f = k\cos\phi, g = k\sin\phi),$$

equation (21) becomes

$$(kB)_k\hat{\Theta}_{\phi\phi} + k\{(kB)\hat{\Theta}_k\}_k = 0, \tag{22}$$

and the Legendre relation (19) simply reads

$$\Theta = k\hat{\Theta}_k - \hat{\Theta}. \tag{23}$$

This section explains how equations (22) and (23) suffice for the construction of exact solutions of (6).

The key reason they do suffice is that equation (22) is separable. With the ansatz

$$\hat{\Theta} = F_n(k)\cos(n\phi + \delta), \tag{24}$$

equation (22) separates, leading for $F_n(k)$ to the ODE

$$k\{(kB)\{F_n\}_k\}_k - n^2(kB)_k\{F_n\} = 0. \tag{25}$$

This separation is a reflection of the rotational invariance of the original phase diffusion equation (6).

The Jacobian (20) of the mapping $(\phi, k) \to (x, y)$ associated with the n^{th} mode solution (24) of equation (22) is

$$J_n = 1 + \cos^2(n\phi)\left[-1 + \frac{(kB)_k}{B}\left(\frac{\{F_n\}_k - \frac{n^2}{k}\{F_n\}}{n\left(\{F_n\}_k - \frac{1}{k}\{F_n\}\right)}\right)^2\right]. \tag{26}$$

Note that along the Eckhaus boundaries where $(kB)_k = 0$, J_n vanishes when $\cos^2(n\phi) = 1$ ($\phi = \frac{m\pi}{n}$), while when $B = 0$, it vanishes for $\cos^2(n\phi) = 0$ ($\phi = \frac{m\pi}{2n}$, m odd).

For $n = 0, 1$, equation (25) admits closed form solutions, which we use to illustrate the general method. For n = 0, the general solution of equation (22) is

$$\hat{\Theta} = a_0 + a_1\int^k \frac{dk}{kB} + a_2\phi + a_3\phi\int^k \frac{dk}{kB}. \tag{27}$$

The mapping from the hodograph plane to the physical plane given by $\vec{X} = (X, Y) = \nabla_{\vec{k}}\hat{\Theta}$ is

$$X = \cos(\phi)\left(\frac{(a_1 + a_3\phi)}{kB}\right) - \frac{\sin(\phi)}{k}\left(a_2 + a_3\int^k \frac{dk}{kB}\right), \tag{28}$$

$$Y = \sin(\phi)\left(\frac{(a_1 + a_3\phi)}{kB}\right) + \frac{\cos(\phi)}{k}\left(a_2 + a_3\int^k \frac{dk}{kB}\right). \tag{29}$$

The pullback of Θ to the hodograph plane, (23), is

$$\Theta = -(a_0 + a_2\phi) + (a_1 + a_3\phi)\left(\frac{1}{B} - \int^k \frac{dk}{kB}\right). \tag{30}$$

The level curves, $\Theta = m\pi$, in the hodograph plane are depicted in Figures 9a–c. The corresponding rolls in the physical plane are calculated by tracing the images of these level curves under the mapping (28) as shown in Figures 9d–f. The patterns represented here are called "vortices" (Fig. 9a,d) in which $\hat{\Theta}$ is a linear function of ϕ, "foci" or "targets" (Fig. 9b,e) in which $\hat{\Theta}$ is purely a function of k, and "spirals" (Fig. 9c,f) which are general n=0 solutions. One can construct spiral solutions with an arbitrary number of arms. If one sets $X = R\cos(\alpha)$, $Y = R\sin(\alpha)$, $k_X = k\cos(\phi)$, and $k_Y = k\sin(\phi)$, then the wavevector gets associated with its physical location by the formulas

$$R = (1/k)\sqrt{a_1^2/B(k)^2 + m^2},$$
$$\alpha = \phi + \tan^{-1}(mB(k)/a_1).$$

Here, m is the number of spiral arms and the parameter a_1 controls the structure of the core of the spiral.

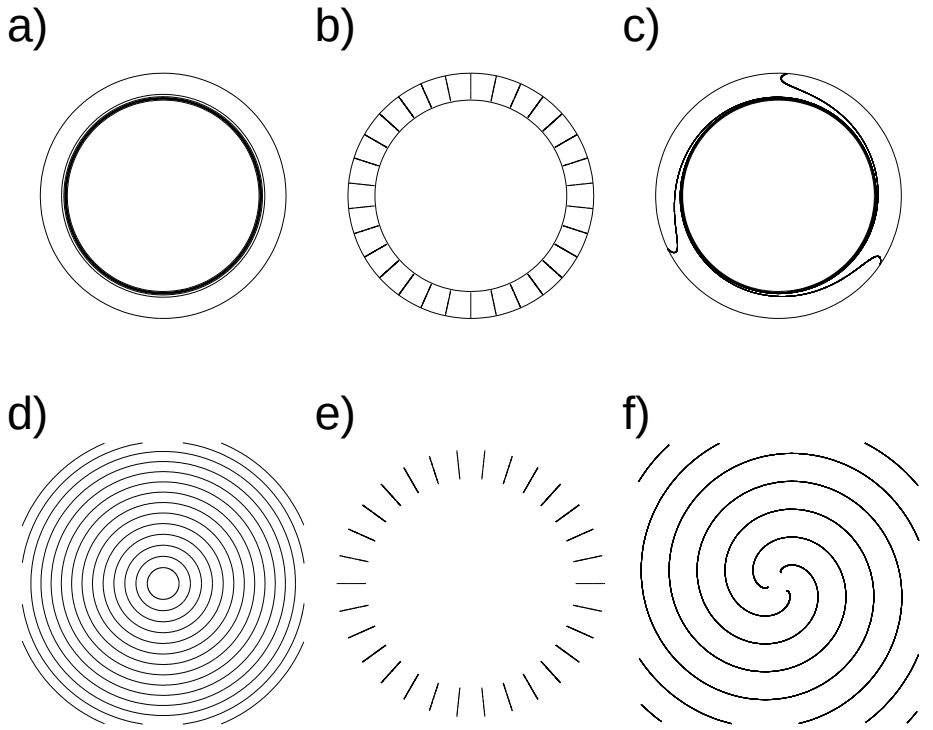

Fig. 9. Contours of $\Theta = m\pi$ for several exactly calculated $n = 0$ solutions in the hodograph plane (a)–(c) and the corresponding contours in the physical plane (d)–(f).

For n = 1 the general solution to equation (22) can be represented as

$$\hat{\Theta} = 2c_1 k \int^k \frac{dk}{k^3 B} \cos(\phi) + c_2 k \cos(\phi - \phi_0), \tag{31}$$

where c_1, c_2 and ϕ_0 are constants and where the rotational degree of freedom corresponding to the substitution $\phi \to \phi + \delta$ has been suppressed. The mapping from the hodograph plane to the physical plane is

$$X = c_1 \int^k \frac{dk}{k^3 B} + \frac{c_1}{k^2 B}(1 + \cos(2\phi)) + c_2 \cos(\phi_0), \tag{32}$$

$$Y = \frac{c_1}{k^2 B} \sin(2\phi) + c_2 \sin(\phi_0). \tag{33}$$

The pullback of Θ to the hodograph plane, (23), is

$$\Theta = \frac{2c}{kB} \cos(\phi). \tag{34}$$

The level curves, $\Theta = m\pi$, in the hodograph plane are depicted in Figure 10a. The corresponding rolls in the physical plane are obtained by tracing the images of these

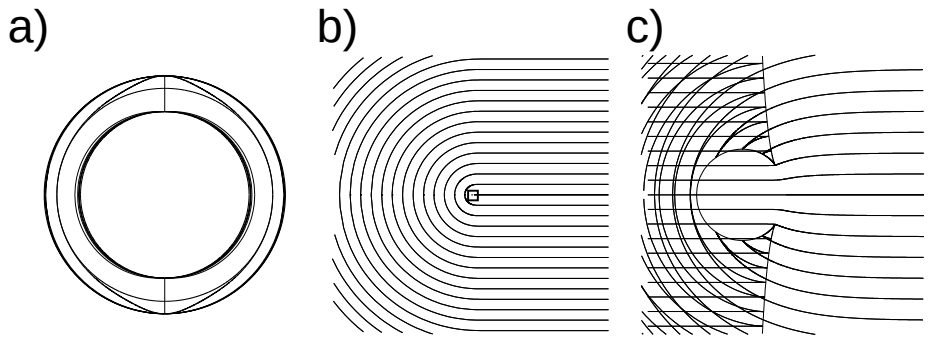

Fig. 10. Contours of $\Theta = m\pi$ for $n = 1$ solution in (a) the hodograph plane and (b) the corresponding contour in the physical plane. A blown-up view of the center (boxed in (b)) with contours drawn for $\Theta = m\pi/10$, and the solution extended out to $k = k_r$, is shown in (c).

level curves under the mapping (32). In Figure 10b we plot the images of these rolls in the physical plane coming from half of a thin annular ring close to $k = k_B (1 < k \leq 1.1, -\frac{\pi}{2} < \phi < \frac{\pi}{2})$.

We refer to the pattern shown here as a "roman arch." There is an apparent defect located near the origin with a half-line emanating from it along which $\vec{k}$ undergoes a jump of π or, equivalently, a reversal of orientation. Parallel to this half-line are apparent straight horizontal rolls with wavelength effectively equal to 1. This part of the pattern comes from the region near $\phi = \pm\frac{\pi}{2}$ in the hodograph plane where in the map (32) the coefficients of the terms proportional to $\frac{1}{B}$ vanish so that the logarithmic term ($\sim \ln(|B|)$) becomes dominant. Assume that $k^2 - 1 = O(\epsilon)$ so that $|B| = O(\epsilon)$; if $|\phi \pm \pi/2| = O(\epsilon)$ then $\sin(2\phi) = O(\epsilon)$ and $1 + \cos(2\phi) = O(\epsilon^2)$ so that

$$X = c \int \frac{dk}{k^3 B} + O(\epsilon), \qquad Y = \frac{c}{k^2 B} \sin(2\phi) = O(1).$$

The Y component is effectively linear in $(\phi \pm \pi/2)/B$, and the X component is effectively independent of ϕ and proportional to $\ln(|B|)$. In the right half of the physical plane the rolls are semicircular. Here the polar part is dominating and the logarithmic integral term in the X component can be neglected.

The image of this narrow ring appears to fill a large open region of the physical plane. In the limit as the inner radius of the ring approaches $k = 1$, the image would appear to fill the entire physical plane. The pointlike defect is a small, roughly circular region in the physical plane. A blowup of this defect region is shown in Figure 10c (same as in Fig. 9a) where the rolls are now level curves $\Theta = m\pi/10$. Within this region is the image of the locus where the jacobian of the mapping (32) vanishes:

$$J_1 = 1 - \cos^2(\phi) \left\{ 1 - \frac{(kB)_k}{B} \right\} = 0. \tag{35}$$

Along this locus (shown in Fig. 10a) the mapping ceases to be 1:1, and its image is a caustic in the physical plane. One sees that the caustic consists of a fold that at two points develops a cusp. Moreover, the rolls themselves develop cusps along the caustic and so

clearly the solution has ceased to be physical. Note that this caustic and the cuspidal rolls all occur in the hyperbolic region beyond the right Eckhaus boundary $k = k_{rE}$.

Equation (25) has a regular singular point at $k = k_B(= 1)$ which is a root of B. Since the energy (7) tends to be minimized by solutions with k uniformly close to k_B, we expect to find good approximations to solutions of the stationary phase diffusion equation from a Frobenius expansion near $k = k_B$ of the solution, $F_n(k)$, to equation (25). Changing variables from k to B, this is equivalent to expanding at $B = 0$. The result to order B^2 is

$$F_n(k) \approx \log|B|(1 + \beta_1 B + \beta_2 B^2) + \gamma_1 B + \gamma_2 B^2,$$

where

$$\begin{aligned}
\beta_1 &= n^2\alpha_1, \\
\beta_2 &= \frac{n^2}{4}\left(4\alpha_2 - \alpha_1^2\left(1 - n^2\right)\right), \\
\gamma_1 &= 2\frac{\alpha_2}{\alpha_1} - \alpha_1\left(1 + 2n^2\right), \\
\gamma_2 &= \frac{\left(6\alpha_3 - (6 + 4n^2)\alpha_1\alpha_2 + (2 + n^2 - 3n^4)\alpha_1^3\right)}{4\alpha_1},
\end{aligned}$$

and if we expand $k \approx 1 + \alpha_1 B + \alpha_2 B^2 + \alpha_3 B^3$ we get

$$\begin{aligned}
\alpha_1 &= -\frac{1}{4R}, \\
\alpha_2 &= -\frac{1}{32R^2}, \\
\alpha_3 &= -\left(\frac{1}{16R^4} + \frac{1}{128R^3}\right),
\end{aligned}$$

where $R = \sqrt{X^2 + Y^2}$.

In this approximation the hodograph map for the "n^{th} mode" is given by

$$\begin{aligned}
\begin{pmatrix} X \\ Y \end{pmatrix} &= \frac{\cos(n\phi)}{\alpha B}\begin{pmatrix} \cos\phi \\ \sin\phi \end{pmatrix} \\
&\quad + n\log|B|\left(n\cos(n\phi)\begin{pmatrix} \cos\phi \\ \sin\phi \end{pmatrix} - \sin(n\phi)\begin{pmatrix} -\sin\phi \\ \cos\phi \end{pmatrix}\right),
\end{aligned} \tag{36}$$

where δ in equation (24) is set to 0 and Θ in the $\vec{k}$ plane is given by

$$\Theta = \left(\frac{1}{\alpha B} + (n^2 - 1)\log|B|\right)\cos(n\phi). \tag{37}$$

Figure 11 shows the rolls in physical ($\vec{X}$) space corresponding to the level curves $\Theta = m\pi$ for a range of m in the case of some small values of n.

The map (36) is a superposition of polar ($\frac{1}{\alpha B}$) and logarithmic ($\log|B|$) terms. When $\cos(n\phi) = 0$, a logarithmic term dominates. In the figures these regions correspond to patches of straight parallel rolls. Note in the figures that these patches occupy a large

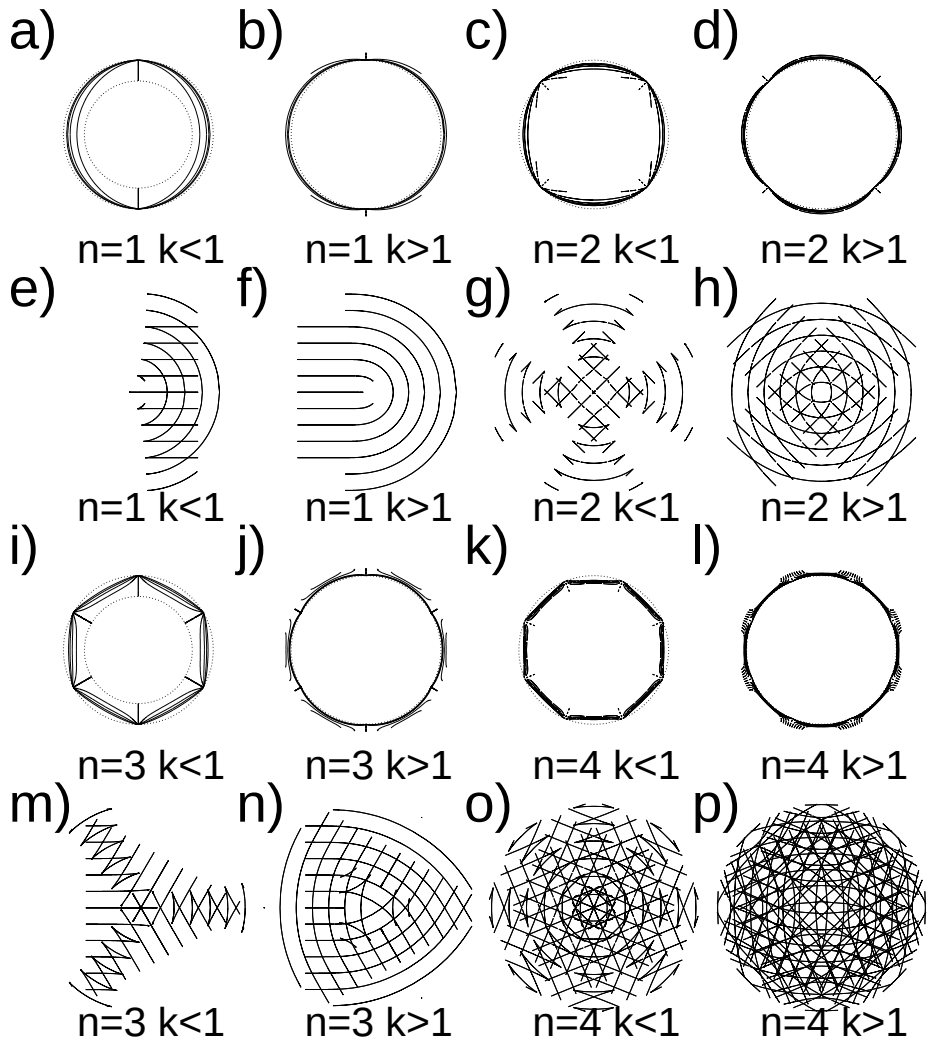

Fig. 11. Rolls in physical plane (e)–(h), (m)–(p) and corresponding pre-images in the *k* plane (a)–(d), (i)–(l).

portion of the $\vec{X}$ plane. On the complement of these patches the polar part is dominant. This is the region of curvature which interpolates the patches of straight rolls.

Again we observe that the figures drawn, which fill infinite sectors of $\vec{X}$ space, are the images of a *very* narrow band of k values near k_B. For $k > k_B$ the defects, which appear pointlike in the figures, correspond to small hyperbolic regions bounded by the image of $|\vec{k}| = k_{rE}$. Outside this small hyperbolic island, the field is elliptic and therefore without folds although the degree of the map is typically greater than 1. For $k < k_B$ the figures are similar with the important exception that now there are folds.

3.3. Weak Solutions of the Stationary Phase Diffusion Equation

In the introduction we displayed several illustrative experimental and numerical patterns (Figures 1, 6, 7, and 8). From these one would expect that the patterns—and their defects—which we want to describe, should correspond to single-valued phase functions, possibly with discontinuities in their derivatives $f = \Theta_X$ and $g = \Theta_Y$. It is natural to ask if one can construct such phase functions from the multivalued solutions we have been considering by "jumping" from one branch of the solution to another along a "shock" as in the classical model of weak solutions to scalar conservation laws. Along a curve in the $\vec{X}$-plane where Θ may have jump discontinuities in its gradient $\vec{k}$, the condition to be a weak solution is

$$\begin{aligned} \vec{k}^{+}_{tang} &= \vec{k}^{-}_{tang}, \\ B\vec{k}^{+}_{norm} &= B\vec{k}^{-}_{norm}, \end{aligned}$$

where $\vec{k}^{\pm}_{tang}$ (resp. $\vec{k}^{\pm}_{norm}$) are the tangential (resp. normal) components on the two sides ($\pm$) of the curve where $\vec{k}$ jumps [51].

A systematic attempt was made to construct weak solutions in the case of 2D stationary ideal isentropic gas dynamics when $B(k^2)$ is the fluid density. There are a number of interesting partial results for this problem (see for instance [17]) but the program was never successfully carried to completion.

One way to satisfy the jump condition for the normal components is if $B = 0$, which occurs, for instance, when $k = 1$. In this case the jump conditions acquire a more symmetrical form since $k = 1$ implies that $(\vec{k}^{\pm}_{tang})^2 + (\vec{k}^{\pm}_{norm})^2 = 1$:

$$\begin{aligned} \vec{k}^{+}_{tang} &= \vec{k}^{-}_{tang}, \\ \vec{k}^{+}_{norm} &= -\vec{k}^{-}_{norm}. \end{aligned} \tag{38}$$

A beautiful example that is almost a weak solution is constructed from the multivalued solution shown in Figure 5c. If one cuts the corresponding surface along the directions of the cube roots of -1, where the rolls cross themselves, then the resulting surface is single-valued with a roll pattern, which is an ideal version of that in Figure 6. The jumps in $\vec{k}$ along the directions of the cube roots of -1 clearly satisfy the jump conditions (38). This is not quite a weak solution since along the jump, B is not identically 0, although it is exponentially close. There is a limiting form of this solution that is a weak solution.

Although one may construct a number of weak solutions in this way, as with the case of gas dynamics, a complete solution seems unlikely. Instead we will take an approach analogous to that of constructing viscosity solutions. In the next section we modify the Cross-Newell equation (6) by adding to it an appropriate regularization term. The solutions of this regularized equation will be smooth and single-valued. In a limit, as the regularization is removed, we expect to recover a single-valued weak solution of (6).

When we consider the limit of regularized solutions we will find that we are driven to limiting weak solutions for which $k = k_B$ almost everywhere. Since, when $k = k_B$, $\lambda_+ = \lambda_-$, this would appear to drive us outside the scope of what we have considered in this section. However, we have seen in the examples of the concave and convex disclinations, that there are branches of multivalued solutions defined on most of the $\vec{X}$ plane for which k is uniformly very close to k_B. We expect the weak limits we study to be closely related to these.* In these examples, the single-valued branch selected by this limit "cuts off" well before the multivalued solution would have reached a caustic. So, caustic singularities are not seen in the weak solution; however, the structure of defects in the weak solution is strongly influenced by the caustics of the associated multivalued solution.

Finally, the point singularities, which for the most part occur at $k = 0$ or ∞ or on the boundaries of caustics, do not appear in limiting weak solutions. However, the twist invariant of these singularities still influences the topology of weak solutions [22].

4. Regularization

The stationary RCN equation (18) is variational. Though not necessary, it will simplify our description to further approximate the energy density (9) to leading order in the vicinity of its minimum $k = k_B = 1$. One then takes $G^2(k) = (1-k^2)^2$, and in this case the free energy for stationary RCN is

$$\mathcal{E}^\epsilon(\Theta) = \int_\Omega \epsilon(\Delta\Theta)^2 \, d\vec{X} + 1/\epsilon \int_\Omega (1-k^2)^2 \, d\vec{X}, \tag{39}$$

where the domain Ω will, from now on, be taken to be a simply connected domain in the plane. In general we consider this energy functional on a class of functions with fixed, though possibly ϵ-dependent, Dirichlet boundary conditions.

Using the null-Lagrangian identity [23], [5],

$$(\Delta\Theta)^2 = |\nabla\vec{k}|^2 + 2[\Theta, \Theta], \tag{40}$$

where $\nabla\vec{k}$ is the matrix of second partial derivatives of Θ, one sees that $\int_\Omega (\Delta\Theta)^2 \, d\vec{X}$

* In fact there do exist solutions of the CN equation for which $k = k_B$ almost everywhere; such solutions have the hodograph jacobian, J, equal to 0 everywhere and correspond to so-called *simple* solutions of the quasilinear system (6) [30].

actually controls the second derivatives in L^2. This follows from (40) because $[\Theta, \Theta]$ is a perfect divergence:
Let $\vec{k} = (f, g)^t$. Then

$$\begin{aligned} 2\int_\Omega [\Theta, \Theta]\, d\vec{X} &= 2\int_\Omega (f_X g_Y - f_Y g_X)\, d\vec{X} && (41)\\ &= \int_\Omega \nabla \cdot \begin{pmatrix} f g_Y - g f_Y \\ g f_X - f g_X \end{pmatrix} d\vec{X} && (42)\\ &= \oint_{\partial\Omega} \vec{k} \times d\vec{k} \\ &= \oint_{\partial\Omega} k^2 d\left(\tan^{-1}\frac{g}{f}\right) \\ &= \oint_{\partial\Omega} k^2(s) d\phi(s). \end{aligned}$$

Thus $\int_\Omega (\Delta\Theta)^2\, d\vec{x}$ may be replaced by $\int_\Omega |\nabla\vec{k}|^2\, d\vec{x}$ in $\mathcal{E}^\epsilon(\Theta)$ at the cost of adding a constant, $c(\epsilon)$, to the energy which depends only on the boundary data:

$$\mathcal{E}^\epsilon(\Theta) = \int_\Omega \epsilon |\nabla\vec{k}|^2\, d\vec{X} + 1/\epsilon \int_\Omega (1 - k^2)^2\, d\vec{X} + c(\epsilon). \tag{43}$$

The minima of this energy are solutions of (18). So one approach to finding single-valued *weak* solutions of the stationary CN equation (6) is to consider a sequence of minimizers Θ^ϵ, one for each ϵ, and describe its limit points, if such exist in an appropriate sense, as $\epsilon \to 0$. Such limit points are referred to as *asymptotic minimizers*. For the boundary conditions we will consider, the constant $c(\epsilon)$ tends to zero as $\epsilon \to 0$ and therefore can be ignored.

The problem of describing the asymptotic minimizers of (43) fits into a natural hierarchy of geometrically and physically motivated singular variational problems. The most basic of these is the *harmonic map problem* [23] which asks to find the minima of

$$\int_\Omega |\nabla\vec{k}|^2\, d\vec{X},$$

where $\vec{k}$ is an arbitrary vectorfield on Ω subject to the constraint that $|\vec{k}| = 1$ and with fixed smooth boundary condition $\vec{k}|_{\partial\Omega} = \vec{g}$ with $|\vec{g}| = 1$. These minimizers are harmonic maps from Ω to S^1. If Ω is simply connected, then minimizers will not exist unless the winding number of $\vec{g}$ around $\partial\Omega$ is zero.

To capture harmonic maps with defects one can weaken the constraint that $|\vec{k}| = 1$ everywhere by incorporating it as a nonconvex term in the variational problem. The energy (43) does this if one takes the domain to be all vectorfields rather than just those which are locally gradient. In this case—that is, when $\vec{k}$ is allowed to range over arbitrary vectorfields—this energy is referred to as the *Ginzburg-Landau* free energy since the gradient flow associated to this energy solves the Ginzburg-Landau equation. It also arises as a model for vortex dynamics in superconductivity [26] and as an idealized model for liquid crystal patterns [39]. One expects that the asymptotic minimizers for this problem should satisfy $|\vec{k}| = 1$ almost everywhere. A complete description of the

asymptotic minimizers for the Ginzburg-Landau problem was recently worked out by Bethuel, Brezis, and Hélein [7]. They showed that if the winding number of $\vec{g}$ around $\partial\Omega$ is $d > 0$, then the asymptotic Ginzburg-Landau minimizers acquire d distinct point defects, at $\vec{a}_1, \ldots, \vec{a}_d$ in the limit, and in the complement these minimizers converge to a harmonic map k_0: $\Omega - \{\vec{a}_1, \ldots, \vec{a}_d\} \to S^1$. The location of the point defects is completely determined by the boundary data $\vec{g}$. The free energy written in microscopic coordinates x, y becomes $\frac{1}{2\epsilon}\mathcal{E}^\epsilon$ with a minimum value that diverges as $\ln \frac{1}{\epsilon}$, where $\frac{1}{\epsilon}$ is the aspect ratio.

The variational problem associated with the RCN equation fits naturally in succession after the previous two. The energy is the Ginzburg-Landau energy but restricted to vectorfields which are gradient. The numerical experiments shown in Figures 6, 7, and 8 suggest that the defects of the asymptotic minimizers occur along one-dimensional curves. For a restricted but interesting class of boundary data our results suggest that away from curvilinear defects the minimizers limit to a smooth viscosity solution of the CN equation associated with the energy density $G^2(k) = (1 - k^2)^2$. In this case the microscopic free energy minimum will diverge as $1/\epsilon$, the aspect ratio.

4.1. Self-Dual Solutions

As mentioned above, equation (6) is a quasilinear second-order differential system which can, depending on wavenumber k, be elliptic or hyperbolic. The time-dependent equation (5) is ill-posed when k crosses into regions where equation (6) becomes hyperbolic. Moreover, in general, classical global stationary solutions will not exist unless they are allowed to be multivalued. We have seen in examples that this occurs when the modulational ansatz is violated and therefore one is led to seek an improved macroscopic model. One such is the regularization (18), which we rewrite here for convenience,

$$\tau(k)\Theta_T + \nabla \cdot \vec{k}B(k) + \epsilon^2\nabla^4\Theta = 0.$$

The regularization term $\epsilon^2\nabla^4_{\vec{X}}\Theta$ is formally order ϵ^2 smaller compared to $\nabla_{\vec{X}} \cdot \vec{k}B(k)$ and only comes into play when k crosses into regions where equation (6) becomes ill-posed and $\nabla_{\vec{X}} \cdot \vec{k}$ can become large on the order of ϵ^{-1}.

Equation (18) can be written as $\tau\Theta_t = -\frac{1}{2}\delta F^\epsilon/\delta\Theta$ with

$$F^\epsilon = \int \left(G^2(|\nabla\Theta|) + \epsilon^2(\nabla^2\Theta)^2\right) dX\, dY, \tag{44}$$

where $G^2 = -\int_{k_B^2}^{k^2} B\, dk^2$ is always nonnegative, with an isolated minimum at $k = k_B$. Note that, in the case of the modulation coefficients for the SH equation (8), for k within the marginal stability band, $\tau(k) > 0$. In fact, this is generally the case [51]. Thus, the linearization of (18) at a stationary solution whose wavenumber support lies within this band, will be pseudo-gradient in the sense that if $\delta F^\epsilon/\delta\Theta > 0$, the stationary solution will be linearly stable with respect to the time evolution.

In introducing higher order terms to regularize the Cross-Newell equation, we lose the method of constructing explicit stationary solutions via the Legendre transform. However, we can, to a certain extent, recover solutions related to this method at least

asymptotically. We refer to this method as *self-dual reduction*.† The idea is motivated by trying to extend to the field-theoretic setting the principle of the equipartition of energy in classical Hamiltonian mechanics in which energy minima occur when the kinetic energy equals the potential energy. In particular, the suggestion that this principle should hold for RCN came from the discovery that it holds exactly in the weak bending setting [44].

In (44), $G^2(k^2)$ is the "potential" and $\epsilon^2\nabla^2\Theta^2$ the "kinetic" energy density. (The analogy for the latter is clearer in the energetically equivalent form $\epsilon|\nabla\vec{k}|^2$ found in (43).) There are results on the equipartition of energy for nonconvex variational problems in the 1D setting [32] as well as in the weak bending setting [44] mentioned above. The method described in this section is generally applicable in 2D problems. This reduction is highly effective as it allows one to exploit the well-developed theory of viscosity solutions to control singular limits.

Let Θ^ϵ_{SD} be a solution of the following second-order equation, which we call the *(anti–)self-dual equation*:

$$\epsilon\nabla^2\Theta^\epsilon_{SD} = \mp G, \tag{45}$$

where G is chosen such that it is positive when $k^2 > k_B^2$.

Proposition 4.1. *A solution of the (anti–)self-dual equation (45) also satisfies*

$$\frac{\delta F^\epsilon}{\delta\Theta} = \pm\epsilon(\nabla^2_{\vec{k}}G)[\Theta,\Theta], \tag{46}$$

where $\frac{1}{2}[\Theta,\Theta] = \det Hess(\Theta) = \Theta_{XX}\Theta_{YY} - \Theta^2_{XY}$.

$$\frac{1}{2}\frac{\delta F^\epsilon}{\delta\Theta} = \epsilon^2\nabla^4\Theta - \nabla(G\nabla_{\vec{k}}G).$$

We separately evaluate the two terms on the RHS. For the first, apply $\epsilon\nabla^2$ to $\epsilon\nabla^2\Theta = sG$, where $s = \pm 1$, to get

$$\begin{aligned}\epsilon^2\nabla^4\Theta &= \epsilon\nabla^2(\epsilon\nabla^2\Theta) = \epsilon\nabla^2(sG) = s\epsilon\nabla\cdot(\nabla_{\vec{X}}G) = s\epsilon\nabla\cdot(\nabla_{\vec{k}}G\cdot Hess(\Theta))\\ &= s\epsilon\frac{\partial}{\partial X}\left(\frac{\partial G}{\partial\Theta_X}\Theta_{XX} + \frac{\partial G}{\partial\Theta_Y}\Theta_{XY}\right) + s\epsilon\frac{\partial}{\partial Y}\left(\frac{\partial G}{\partial\Theta_X}\Theta_{XY} + \frac{\partial G}{\partial\Theta_Y}\Theta_{YY}\right).\end{aligned}$$

For the second term we have, using equation (45),

$$\begin{aligned}\nabla(G\nabla_{\vec{k}}G) &= s\epsilon\nabla(\nabla^2\Theta\nabla_{\vec{k}}G)\\ &= s\epsilon\frac{\partial}{\partial X}\left((\Theta_{XX}+\Theta_{YY})\frac{\partial G}{\partial\Theta_X}\right) + s\epsilon\frac{\partial}{\partial Y}\left((\Theta_{XX}+\Theta_{YY})\frac{\partial G}{\partial\Theta_Y}\right).\end{aligned}$$

Taking the difference of these terms we find that

$$\frac{1}{2}\frac{\delta F^\epsilon}{\delta\Theta} = -s\epsilon\left(\frac{\partial^2 G}{\partial\Theta_X^2} + \frac{\partial^2 G}{\partial\Theta_Y^2}\right)\left(\Theta_{XX}\Theta_{YY} - \Theta^2_{XY}\right).$$

† The term *self-dual* is borrowed from quantum field theory. This concept is used to achieve a reduction from fourth to second order in the Yang-Mills field equations [26]. There, as here, the reduction is effected by making the ansatz (45) of energy equipartition.

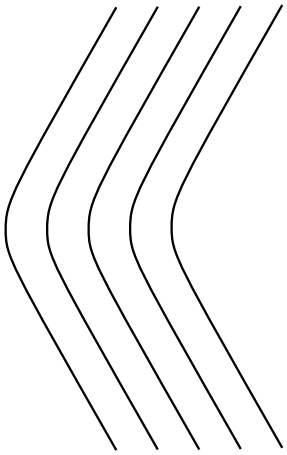

Fig. 12. "Knee" solution of self-dual equation.

Proposition 4.1 shows that a solution of equation (45) is a critical point of the free energy *if* $[\Theta, \Theta]$ is also zero. Since $[\Theta, \Theta]$ is proportional to the curvature of the surface which is the graph of Θ, we can also interpret this as saying that curvature measures the deviation of (anti–)self-dual solutions from being solutions of the variational equations. This result does *not* tell us that Θ^{ϵ}_{SD} minimizes F^{ϵ}. However, in the next section we will demonstrate, for an interesting class of self-dual solutions, that asymptotically they limit to weak solutions of the unregularized phase diffusion equation that in an appropriate sense are asymptotic minimizers of F^{ϵ} as $\epsilon \to 0$.

4.2. Viscosity Solutions of the Self-Dual Equation

When k is near k_B, $G = k^2 - k_B^2$ to a good approximation. From now on we will take $k_B = 1$. When k is close to 1, we replace G by $k^2 - 1$ and then the (anti–)self-dual equation (45) may be transformed to a linear equation, in fact the Helmholtz equation,

$$\epsilon^2 \nabla^2 \psi - \psi = 0 \tag{47}$$

by the logarithmic transformation $\Theta = \pm\epsilon \ln \psi$.

An illustrative and important example of the method of self-dual reduction is provided by what we refer to as a "knee" solution of (47) (see Figure 12) which models a defect along a one-dimensional contour (called a *phase grain boundary* in the literature on pattern formation):

$$\Theta = k_0 X - \varepsilon \ln 2 \cosh \left(\sqrt{1 - k_0^2}\, Y/\varepsilon \right). \tag{48}$$

It is straightforward to check that this solution in fact solves equation (18) since $[\Theta, \Theta] \equiv 0$. This solution can also be interpreted in the following way: The zig-zag instability of the field of rolls $\Theta = k_0 X$ with wavevector $(k_0, 0)$, $k_0 < 1$, saturates into

a pair of roll fields $(k_0, +\sqrt{1-k_0^2})$ and $(k_0, -\sqrt{1-k_0^2})$ separated by a boundary layer along the bisector of their constant phase contours. The asymptotic limit of (48) as $\epsilon \to 0$ is a weak solution of the CN equation (see Section 3.3).

Now more generally let $\Psi^{(\epsilon)}(\vec{X})$ be any classical solution of the Helmholtz equation (47) on a bounded domain Ω with smooth boundary and with Dirichlet boundary conditions:

$$\Psi^{(\epsilon)}(\vec{X}(s)) = v^{(\epsilon)}(s),$$

where $v^{(\epsilon)}(s)$ is continuous and piecewise differentiable along $\partial\Omega$ for each ϵ and $\vec{X}(s)$ denotes the arclength parametrization of $\partial\Omega$.

We will assume that the sequence $v^{(\epsilon)}(s)$ converges uniformly in ϵ to a continuous function $v^{(0)}(s)$ on $\partial\Omega$ and that

$$\lim_{\epsilon\to 0} \epsilon \left(\nabla \log \Psi^{(\epsilon)}\right)(\vec{X}(s)) \cdot \hat{n}(s) = \beta^{(0)}(s), \tag{49}$$

where $\beta^{(0)}(s)$ is continuous and where we have denoted the outward unit normal to $\partial\Omega$ by $\hat{n}(s)$.

In the case when $v^{(\epsilon)}(s)$ is a constant independent of ϵ, which physically corresponds to $\partial\Omega$ being a roll, the following result of Ishii and Koike [25] enables us to show that assumption (49) is valid.

Theorem 4.2. *For $v^{(\epsilon)}(s) \equiv 1$ and $\epsilon > 0$, let Ψ^{ϵ} be the solution of (47). Then*

(a) *there is a constant $C_1 > 0$ such that*

$$|\epsilon \log \Psi^{\epsilon}(\vec{X}) - d(\vec{X})| \le C_1 \epsilon^{1/2},$$

for $\vec{X} \in \Omega$ and $\epsilon > 0$, where $d(\vec{X})$ is the distance from $\vec{X}$ to $\partial\Omega$.

(b) *there is a constant $C_2 > 0$ such that*

$$|\Theta(\vec{X}) - \Theta(\vec{Y})| \le C_2 |\vec{X} - \vec{Y}|,$$

for $(\vec{X}, \vec{Y}) \in \partial(\Omega \times \Omega)$ and $\epsilon > 0$.

Briefly, the proof of this theorem proceeds as follows. First, one derives a continuous upper bound, independent of ϵ. Define

$$V(x) = \sup\{\Theta^{\epsilon}(x) : 0 < \epsilon < 1\},$$

for $x \in \bar{\Omega}$, and

$$V^*(x) = \lim_{r\to 0} \sup\left\{V(y):\ y \in \bar{\Omega},\ |y - x| \le r\right\}.$$

The function V^* is manifestly an upper bound independent of ϵ. Using obstacle functions, Ishii and Koike prove that this function is Lipshitz. It follows from the maximum principle

that $\Theta^\epsilon(x)$ is nonnegative on $\bar{\Omega}$. Part (b) of the theorem is immediate from these two observations.

From (a) we have that the sequence $\epsilon \log \Psi^\epsilon(\vec{X})$ converges uniformly to the distance function and (b) implies that the condition on the normal derivatives, (49), holds. Once condition (49) is known to hold, the following asymptotic analysis determines the limits of the higher derivatives $\vec{k}$ and $\nabla\vec{k}$ as well.

Using Green's identity [14], one has a boundary integral representation

$$\Psi^{(\epsilon)}(\vec{X}) = \int_{\partial\Omega} v^\epsilon(\vec{Y}(s)) \frac{\partial G^{(\epsilon)}}{\partial n}(\vec{X}, \vec{Y}(s)) - G^{(\epsilon)}(\vec{X}, \vec{Y}(s)) \frac{\partial v^\epsilon(\vec{Y}(s))}{\partial n}\, ds, \tag{50}$$

where $G^{(\epsilon)}$ is the Green's function for the Helmholtz equation on all of $\mathbb{R}^2$:

$$G^{(\epsilon)}(\vec{X}, \vec{Y}) = -\frac{1}{2\pi} K_0\left(\frac{|\vec{X} - \vec{Y}|}{\epsilon}\right),$$

for $\vec{X}$ in the interior of Ω. The modified Bessel functions of integer order, $K_n(r)$ [1], formula 9.7.2, all have a singular point at $r = 0$ and large r asymptotics

$$K_n(r) \approx \sqrt{\frac{\pi}{2r}} e^{-r} \left\{1 + \frac{4n^2 - 1}{8r}\right\}. \tag{51}$$

From [1], formula 9.6.27, we also have the useful relation

$$K_1(r) = -\frac{d}{dr} K_0(r), \tag{52}$$

and

$$K_0(r) + \frac{1}{r} K_1(r) = -\frac{d}{dr} K_1(r). \tag{53}$$

Substituting (52) and (51) into (50),

$$\begin{aligned}
\Psi^{(\epsilon)}(\vec{X}) \;=\; & \frac{1}{2\pi} \int_{\partial\Omega} \frac{v^\epsilon(s)}{\epsilon} K_1\left(\frac{|\vec{X} - \vec{Y}(s)|}{\epsilon}\right) \left(\frac{\vec{Y}(s) - \vec{X}}{|\vec{Y}(s) - \vec{X}|} \cdot \hat{n}\right) \\
& + \frac{\partial v^\epsilon}{\partial n}(s) K_0\left(\frac{|\vec{X} - \vec{Y}(s)|}{\epsilon}\right) ds \\
= \; & \frac{1}{2\pi} \int_{\partial\Omega} \left(\frac{v^\epsilon(s)}{\epsilon} \frac{\vec{Y}(s) - \vec{X}}{|\vec{Y}(s) - \vec{X}|} \cdot \hat{n} + \frac{\partial v^\epsilon}{\partial n}(s)\right) \\
& \cdot \left(\sqrt{\frac{\pi\epsilon}{2|\vec{X} - \vec{Y}(s)|}} \exp\left(-\frac{|\vec{X} - \vec{Y}(s)|}{\epsilon}\right)\right)_{\vec{Y} = \vec{Y}(s)} \\
& + \mathcal{O}\left(\sqrt{\frac{\epsilon}{|\vec{X} - \vec{Y}(s)|}} \exp\left(\frac{-|\vec{X} - \vec{Y}(s)|}{\epsilon}\right)\right) ds.
\end{aligned} \tag{54}$$

In addition, applying (53) and (51) to the gradient of (50) gives

$$\begin{aligned}\nabla\Psi^{(\epsilon)}(\vec{X}) &= \frac{1}{2\pi}\int_{\partial\Omega}\frac{v^\epsilon(s)}{\epsilon}K_0\left(\frac{|\vec{X}-\vec{Y}(s)|}{\epsilon}\right)\left(\frac{\vec{Y}(s)-\vec{X}}{|\vec{Y}(s)-\vec{X}|}\cdot\hat{n}\right)\left(\frac{\vec{Y}(s)-\vec{X}}{|\vec{Y}(s)-\vec{X}|}\right)\\ &\quad+\frac{\epsilon}{|\vec{X}-\vec{Y}(s)|}K_1\left(\frac{|\vec{X}-\vec{Y}(s)|}{\epsilon}\right)\left(\frac{\vec{Y}(s)-\vec{X}}{|\vec{Y}(s)-\vec{X}|}\cdot\hat{n}\right)\left(\frac{\vec{Y}(s)-\vec{X}}{|\vec{Y}(s)-\vec{X}|}\right)\\ &\quad+\frac{\partial v^\epsilon}{\partial n}(s)K_1\left(\frac{|\vec{X}-\vec{Y}|}{\epsilon}\right)\left(\frac{\vec{Y}(s)-\vec{X}}{|\vec{Y}(s)-\vec{X}|}\right)ds\\ &= \frac{1}{2\pi}\int_{\partial\Omega}\left(\frac{v^\epsilon(s)}{\epsilon}\frac{\vec{Y}(s)-\vec{X}}{|\vec{Y}(s)-\vec{X}|}\cdot\hat{n}+\frac{\partial v^\epsilon}{\partial n}(s)\right)\\ &\quad\cdot\left(\sqrt{\frac{\pi\epsilon}{2|\vec{X}-\vec{Y}(s)|}}\exp\left(-\frac{|\vec{X}-\vec{Y}(s)|}{\epsilon}\right)\left(\frac{\vec{Y}(s)-\vec{X}}{\epsilon|\vec{Y}(s)-\vec{X}|}\right)\right)_{\vec{Y}=\vec{Y}(s)}\\ &\quad+\mathcal{O}\left(\left(\frac{\epsilon}{|\vec{X}-\vec{Y}(s)|}\right)^{3/2}\exp\left(\frac{-|\vec{X}-\vec{Y}(s)|}{\epsilon}\right)\right)ds.\end{aligned}\tag{55}$$

The self-dual boundary data Θ^ϵ is expressed as Helmholtz data through

$$v^\epsilon(s)=\exp\left(\frac{1}{\epsilon}\Theta^\epsilon(\vec{Y}(s))\right).\tag{56}$$

Replacing $v^\epsilon(s)$ by (56) and substituting this into (54), one then arrives at the asymptotic representation

$$\begin{aligned}\Psi^{(\epsilon)}(\vec{X}) &= \frac{1}{2^{3/2}\sqrt{\pi\epsilon}}\int_{\partial\Omega}\left(\frac{\vec{X}-\vec{Y}(s)}{|\vec{X}-\vec{Y}(s)|}-\nabla\Theta(\vec{Y}(s))\right)\\ &\quad\cdot\hat{n}(s)\exp\left(-\frac{|\vec{X}-\vec{Y}(s)|-\Theta(\vec{Y}(s))}{\epsilon}\right)ds\\ &\quad+\mathcal{O}\left(\sqrt{\epsilon}\exp\left(\frac{-d(\vec{X})}{\epsilon}\right)\right),\end{aligned}\tag{57}$$

where $d(\vec{X})$ is the distance from $\vec{X}$ to $\partial\Omega$, $\hat{n}(s)=\binom{-Y_2'(s)}{Y_1'(s)}$ and we have used the substitution

$$\frac{\partial v^\epsilon}{\partial n}(s)\frac{1}{v^\epsilon(s)}=\beta^{(0)}(s)=\nabla\Theta(\vec{Y}(s))\cdot\hat{n}.$$

Note that in this last point we have used the assumption (49) which, if valid, insures that $\beta^{(0)}(s)$ is $\mathcal{O}(1)$ in ϵ so that (57) is a valid asymptotic representation.

Similarly, we see that

$$\begin{aligned}\nabla\Psi^{(\epsilon)}(\vec{X}) \;=\; & \frac{1}{2^{3/2}\sqrt{\pi\epsilon^3}}\int_{\partial\Omega}\left(\frac{\vec{X}-\vec{Y}(s)}{|\vec{X}-\vec{Y}(s)|}-\nabla\Theta(\vec{Y}(s))\right)\cdot\hat{n}(s) \\ & \cdot\exp\left(-\frac{|\vec{X}-\vec{Y}(s)|-\Theta(\vec{Y}(s))}{\epsilon}\right)\left(\frac{\vec{Y}(s)-\vec{X}}{|\vec{Y}(s)-\vec{X}|}\right)ds \\ & +\mathcal{O}\left(\frac{1}{\sqrt{\epsilon}}\exp\left(\frac{-d(\vec{X})}{\epsilon}\right)\right).\end{aligned} \tag{58}$$

Asymptotically for small ϵ, the dominant contribution in these integrals comes from places on the boundary at which the exponent $|\vec{X}-\vec{Y}(s)|-\Theta(\vec{Y}(s))$ is minimal. For most $\vec{X}$ there will be a unique simple minimum $\bar{s}$. In this case (later we will discuss what happens when the minimum is not unique), the dominant contribution can be evaluated by Laplace's method and gives, to leading order in ϵ,

$$\begin{aligned}\Psi^{(\epsilon)}(\vec{X}) \;=\; & \frac{1}{4}\left(\left|\left(|\vec{X}-\vec{Y}(\bar{s})|-\Theta(\vec{Y}(\bar{s}))\right)''\right|\right)^{-1/2} \\ & \left(\frac{\vec{X}-\vec{Y}(\bar{s})}{|\vec{X}-\vec{Y}(\bar{s})|}-\nabla\Theta(\vec{Y}(\bar{s}))\right)\cdot\hat{n}(\bar{s})\exp\left(-\frac{|\vec{X}-\vec{Y}(\bar{s})|-\Theta(\vec{Y}(\bar{s}))}{\epsilon}\right) \\ & +\mathcal{O}\left(\sqrt{\epsilon}\exp\left(\frac{d(\vec{X})}{\epsilon}\right)\right).\end{aligned} \tag{59}$$

The asymptotic phase gradient is then

$$\epsilon\frac{\nabla\Psi^{\epsilon}}{\Psi^{\epsilon}}=\vec{k}^{\epsilon}(\vec{X})=\vec{k}^{(0)}(\vec{X})+\mathcal{O}(\epsilon), \tag{60}$$

with

$$\vec{k}^{(0)}(\vec{X})=\lim_{\epsilon\to 0}\epsilon\nabla_{\vec{X}}\log\Psi^{\epsilon}(\vec{X})=\frac{\vec{X}-\vec{Y}(\bar{s})}{|\vec{X}-\vec{Y}(\bar{s})|}, \tag{61}$$

where $\bar{s}$ satisfies

$$\left(\frac{\vec{X}-\vec{Y}(\bar{s})}{|\vec{X}-\vec{Y}(\bar{s})|}+\nabla\Theta(\vec{Y}(\bar{s}))\right)\cdot\vec{Y}\,'(\bar{s})=0, \tag{62}$$

and $\vec{Y}\,'(\bar{s})$ is the unit tangent vector to the boundary at $\bar{s}$. Since the integrand in (57) is uniformly bounded for $\vec{X}\in\Omega$, this representation can be differentiated arbitrarily. In particular, tracking the asymptotic representation of $\nabla\Psi$ as was done for Ψ itself yields that for points $\vec{X}$ at which the phase $|\vec{X}-\vec{Y}(s)|-\Theta(\vec{Y}(s))$ has a unique minimum

$$\nabla\vec{k}^{\epsilon}(\vec{X})=\nabla\vec{k}^{(0)}(\vec{X})+\mathcal{O}(\epsilon), \tag{63}$$

where $\nabla\vec{k}$ is the matrix of second partial derivatives of Θ.

At points $\vec{X}$ where Laplace's method yields a unique minimum, this minimum value is also unique in a neighborhood of $\vec{X}$ and varies smoothly in this neighborhood. Therefore, $\vec{X}$ is not part of a defect. Defects occur at points $\vec{X}_0$ where there are two or more critical points, $\bar{s}_1, \bar{s}_2, \ldots$, for which $|\vec{X}_0 - \vec{Y}(\bar{s}_i)| - \Theta(\vec{Y}(\bar{s}_i))$ attains the *same* minimal value. We include in this the possibility that a defect occurs with multiplicity two or more; i.e., as a consequence of the coalescence of two or more simple defects.

Using equation (61) one sees that $\vec{k}^{(0)}(\vec{X})$ has magnitude 1 everywhere, and therefore the corresponding $\Theta^{(0)}$ is a ruled surface away from defects. Consequently, $[\Theta^{(0)}, \Theta^{(0)}] = 0$ and so away from possible defects we in fact have a solution of the limiting equation (6).

For a given $\vec{X}_0$, the condition that there are exactly two critical points attaining the same minimum value imposes one condition on $\vec{X} \in \Omega$. Hence there is a curve in the interior of Ω (depicted in Figure 13c as the curve separating the regions labeled α and β) containing $\vec{X}_0$ such that over this curve two branches (Figure 13a) of a multivalued solution of equation (6) intersect. These two branches are associated with the two critical points $\bar{s}_\alpha, \bar{s}_\beta$. The roll pattern near this defect consists of almost equally spaced level curves of the single-valued truncation (Figure 13b) of the multi-valued solution of (6). We call such curves *grain boundaries*. These grain boundaries will persist under perturbations of the boundary data. Roughly speaking, a perturbation will slightly move the two intersecting branches but the new branches will still intersect transversely.

The following proposition shows that along grain boundaries, $\vec{k}^{(0)}$ satisfies the same jump conditions (38) as weak solutions of (6).

Proposition 4.3. *Let Γ denote a grain boundary. For $\vec{X} \in \Gamma$*

$$\begin{aligned} \vec{k}^0_{tang}(\vec{X}|\bar{s}_1) &= \vec{k}^0_{tang}(\vec{X}|\bar{s}_2), \\ \vec{k}^0_{norm}(\vec{X}|\bar{s}_1) &= -\vec{k}^0_{norm}(\vec{X}|\bar{s}_2), \end{aligned}$$

where $\vec{k}^0_{tang}(\vec{X}|\bar{s}_i)$ (resp. $\vec{k}^0_{norm}(\vec{X}|\bar{s}_i)$) is the tangential (resp. normal) component along Γ of $\vec{k}^0$ corresponding to the boundary point $\bar{s}_i$. In other words, the jump in $\vec{k}^0$ along Γ is normal to Γ.

This follows by a direct calculation from the condition that

$$|\vec{X} - \vec{Y}(\bar{s}_1)| - \Theta(\vec{Y}(\bar{s}_1)) = |\vec{X} - \vec{Y}(\bar{s}_2)| - \Theta(\vec{Y}(\bar{s}_2))$$

and from the variational condition (62).

For a given $\vec{X}_0$, the condition that there are exactly three critical points attaining the same minimum value imposes two conditions on $\vec{X} \in \Omega$. Hence there is a discrete set of points where three branches of a multivalued Θ intersect. We refer to these points as *spines*; each such point will be a place where three grain boundaries $\bar{s}_\alpha, \bar{s}_\beta$, and $\bar{s}_\gamma$ of Θ coincide. Figure 14 illustrates how a spine defect arises from these three branches.

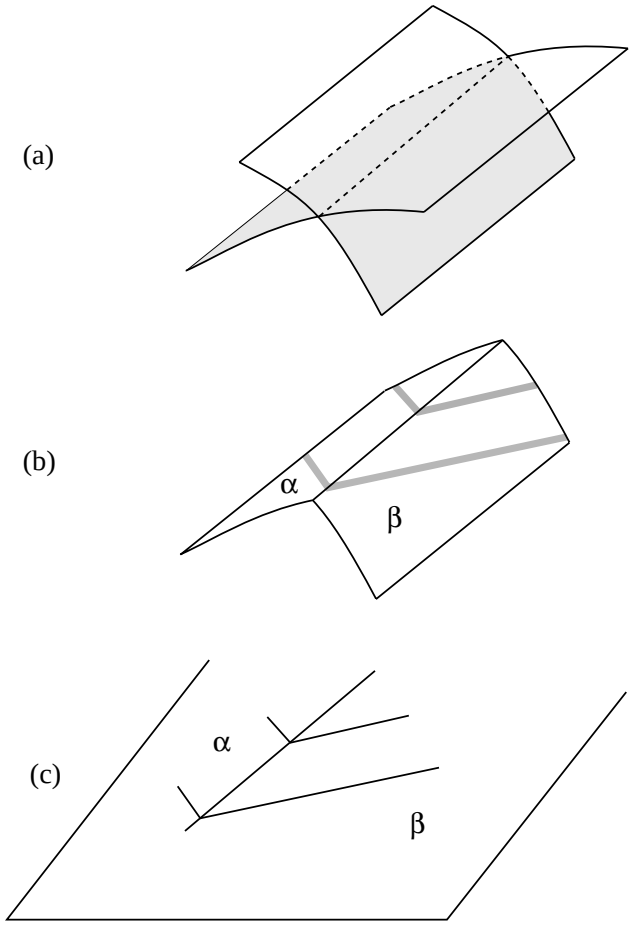

Fig. 13. Grain boundary constructed by Laplace's method from a self-dual solution.

These point defect configurations will be topologically stable under perturbation of the boundary data. A perturbation will move the three intersecting branches but the new branches will still intersect transversely at a new point.

When

$$\left(|\vec{X} - \vec{Y}(\bar{s})| - \Theta(\vec{Y}(\bar{s}))\right)'' = 0, \tag{64}$$

the Laplace representation needs to be replaced by a different asymptotic representation, whose normal form is a Pearcey integral [3]. This occurs when, as $\vec{X}$ varies along a grain boundary, the two critical points $\bar{s}_1, \bar{s}_2$ with the same critical value coincide. Generically at such a point the grain boundary terminates. Therefore we refer to such points as *terminal points*.

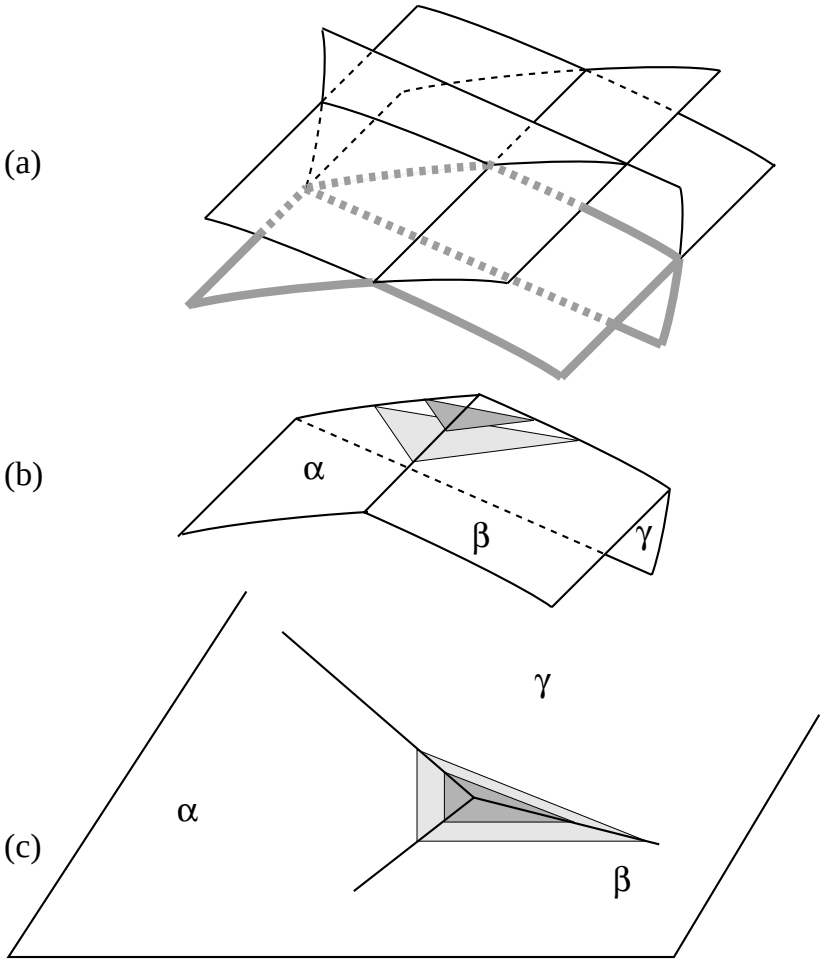

Fig. 14. Spine constructed by Laplace's method from a self-dual solution.

If Θ is constant on $\partial\Omega$, then (64) becomes

$$\frac{1}{|\vec{X}-\vec{Y}(\bar{s})|}-\frac{\vec{X}-\vec{Y}(\bar{s})}{|\vec{X}-\vec{Y}(\bar{s})|}\cdot\vec{Y}''(\bar{s})=0.$$

The second term is the expression for the inverse of the curvature of $\partial\Omega$ at $\bar{s}$. Thus the degeneracy condition (64) has the interpretation that $\vec{X}$ is the center of curvature for a point $\vec{y}(\bar{s})$ where the curvature of $\partial\Omega$ has a local maximum. This is shown in Figure 15. Note in this figure that there is a sharp transition from smooth rolls to a shock that occurs precisely at the center of curvature.

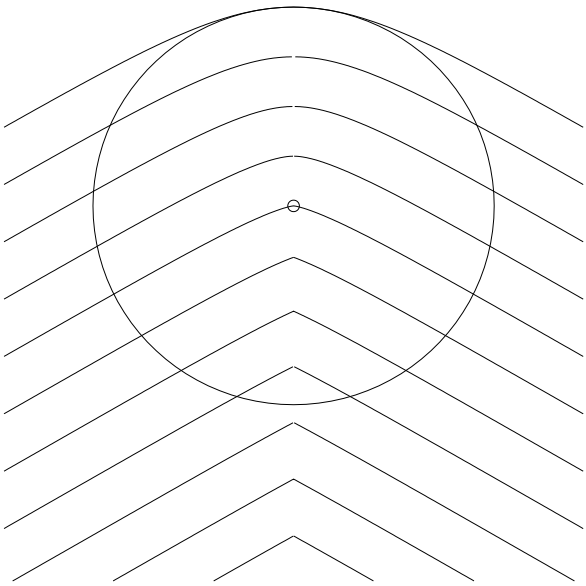

Fig. 15. Terminal point constructed by Laplace's method from a self-dual solution.

The asymptotic behavior of the boundary integral (57) in the vicinity of a terminal point is given by

$$\begin{aligned}\Psi^{(\epsilon)}(\vec{X}) \;=\; & \epsilon^{-1/6}\frac{\Gamma(1/3)}{6^{2/3}\sqrt{8\pi}}\left(\left|\left(|\vec{X}-\vec{Y}(\bar{s})|-\Theta(\vec{Y}(\bar{s}))\right)'''\right|\right)^{-1/3}\\ & \times\left(\frac{\vec{X}-\vec{Y}(\bar{s})}{|\vec{X}-\vec{Y}(\bar{s})|}-\vec{k}(\vec{Y}(\bar{s}))\right)\cdot\hat{n}(\bar{s})\exp\left(-\frac{|\vec{X}-\vec{Y}(\bar{s})|-\Theta(\vec{Y}(\bar{s}))}{\epsilon}\right)\\ & +\mathcal{O}\left(\epsilon^{5/6}\exp\left(\frac{-1}{\epsilon}\right)\right).\end{aligned} \tag{65}$$

Assumption (49) still insures that $\vec{k}(\vec{Y}(\bar{s}))\cdot\hat{n}$ is $\mathcal{O}(1)$ so that this asymptotic is valid. Although this differs from (59), the phase gradient near a terminal point still has an asymptotic representation of the form of (60) and (63).

The topological stability of these singularities for the phase diffusion equation is also easy to see in the case when Θ is constant on $\partial\Omega$; in this case equation (64) is equivalent to $\vec{X}$ being the center of curvature for a point $\vec{Y}(\bar{s})$ where the curvature of $\partial\Omega$ has a local maximum.

If the boundary data is perturbed, a convex "focus" will persist, slightly removed from the curvature center of the boundary. This is not a convex disclination unless the jump in the inclination of $\vec{k}$ across the grain boundary is equal to π.

The types of defects we have just described are, generically, the only types one will see:

Theorem 4.4. *For generic boundary data* $v^{(\epsilon)}(s) = \exp(\frac{1}{\epsilon}\Theta(\vec{Y}(s)))$ *satisfying (49), the viscosity limit* ($\epsilon \to 0$) *of the solution of the Helmholtz boundary value problem* $\Psi^{(\epsilon)}(s)$ *has level curves (roll pattern) whose defects consist of only grain boundaries that branch at spines and terminate at terminal points.*

The proof of this result, given in [3] or [20], essentially follows the lines of the arguments sketched above [22].

In the next section we will discuss how to show that these limiting (as $\epsilon \to 0$) self-dual solutions are in fact realized as limits of stationary solutions of the regularized phase diffusion equation (18). However, since these solutions arise as limits of solutions whose gradient fields are in fact global vectorfields, the limits cannot have odd twist. In particular, these limits cannot realize concave or convex disclinations. To achieve this one needs to build multivaluedness into the boundary conditions. If this is done, then by the results of [13] one finds the concave and convex disclinations are generic as well. One can study these types of defects with single-valued boundary conditions by constructing special boundaries which support an *even* number of disclinations in the interior of Ω. We will look at an example of this in the next section by considering a stadium shaped region which supports two convex disclinations connected by a straight grain boundary.

5. Asymptotics of Minimizers

In the previous section we saw that the self-dual solutions captured the correct behavior of critical points of the free energy at least away from defects. We will see that the self-dual solutions can also asymptotically capture the correct behavior of *minimizers* in the vicinity of defects. In this section we are going to examine the asymptotic behavior of the free energy in a restricted but nevertheless representative class of examples.

We recall that the free energy (44) for the regularized phase diffusion equation in the case when $G^2(k) = (1-k^2)^2$ is, when multiplied by $2\epsilon^{-1}$, given by

$$\mathcal{E}^{\epsilon}(\Theta) = \int_{\Omega} \epsilon(\Delta\Theta)^2 \, d\vec{X} + 1/\epsilon \int_{\Omega} (1-k^2)^2 \, d\vec{X}, \tag{66}$$

where the domain Ω will, from now on, be taken to be a simply connected domain in the plane. In general we consider this energy functional on a class of functions with fixed Dirichlet boundary conditions:

$$\mathcal{A}^{\epsilon} = \left\{ \Theta \in H^2(\Omega) : \Theta|_{\partial\Omega} = \alpha^{\epsilon}(s), \frac{\partial\Theta}{\partial n}|_{\partial\Omega} = \beta^{\epsilon}(s) \right\}, \tag{67}$$

where $\alpha^{\epsilon}(s)$ and $\beta^{\epsilon}(s)$ are both piecewise smooth functions on the boundary parameterized with respect to arclength s. We also recall from (43) in Section 4 that the free energy is equivalent to

$$\mathcal{E}^{\epsilon}(\Theta) = \int_{\Omega} \epsilon|\nabla\vec{k}|^2 \, d\vec{X} + 1/\epsilon \int_{\Omega} (1-k^2)^2 \, d\vec{X} + c(\epsilon). \tag{68}$$

Standard arguments [23] show that for $\epsilon > 0$, $\mathcal{E}^\epsilon$ realizes a minimum in $\mathcal{A}^\epsilon$ and that any such minimizer is smooth. However, for functionals of this class, it is *not* known whether there is a unique minimizer [38]. Nevertheless, if $\{\Theta^\epsilon\}$ is a sequence of such minimizers, one can investigate properties of its limit points.

For the function classes, $\mathcal{A}^\epsilon$, that we will consider, α^ϵ and β^ϵ will be chosen so that as $\epsilon \to 0$, $k^2 = \dot{\alpha}^2 + \beta^2 \to 1$ everywhere along the boundary of Ω. In this case $c(\epsilon)$, defined in (41), limits to a purely topological invariant of the boundary data:

$$\lim_{\epsilon \to 0} c(\epsilon) = \oint_{\partial\Omega} d\phi(s) = \text{ winding number of } \vec{k} \text{ around } \partial\Omega.$$

We are going to compare the minimizers $\{\Theta^\epsilon\}$ to the (anti–)self-dual solutions discussed in Section 4. Since the (anti–)self-dual equations are second order, their solutions are already determined by specifying $\Theta|_{\partial\Omega} = \alpha^\epsilon(s)$. We denote the self-dual solution corresponding to $\alpha^\epsilon(s)$ by Θ^ϵ_{SD}. Then we will take $\beta^\epsilon(s) = \partial_n \Theta^\epsilon_{SD}|_{\partial\Omega}$. With this choice of $\beta^\epsilon(s)$, Θ^ϵ_{SD}, which is smooth and hence in $H^2(\Omega)$, lies in the admissible class $\mathcal{A}^\epsilon$. This condition on $\beta^\epsilon(s)$ is not as restrictive as it might at first seem since our model is derived in a regime where $k \approx 1$. It follows from (61) that, in the limit as $\epsilon \to 0$, $\dot{\alpha}^2 + \beta^2 \to 1$ and, therefore, as mentioned above, the boundary integral (41) tends to a purely topological invariant of the boundary data.

The previous paragraph sets the stage for the principal application of (anti–)self-dual solutions to the description of asymptotic minimizers. Namely, since $\Theta^\epsilon_{SD} \in \mathcal{A}^\epsilon$, and Θ^ϵ minimizes the energy we must have

$$\mathcal{E}^\epsilon(\Theta^\epsilon) \leq \mathcal{E}^\epsilon(\Theta^\epsilon_{SD}). \tag{69}$$

We will see, in Corollary 5.5 that the RHS of (69) is uniformly bounded in ϵ.

We begin our analysis of the free energy by rewriting it as follows:

$$\begin{aligned} \mathcal{E}^\epsilon(\Theta) &= \int_\Omega \left(\epsilon^{1/2}(\nabla \cdot \vec{k}) + \epsilon^{-1/2}(1-k^2)\right)^2 d\vec{X} \\ &\quad - 2\int_\Omega (\nabla \cdot \vec{k})(1-k^2)\, d\vec{X} \qquad (70) \\ &= \int_\Omega \left(\epsilon^{1/2}(\nabla \cdot \vec{k}) + \epsilon^{-1/2}(1-k^2)\right)^2 d\vec{X} \\ &\quad - 2\oint_{\partial\Omega} (1-k^2)\vec{k} \cdot \hat{n} ds - 4\int_\Omega \vec{k} \cdot \nabla\vec{k} \cdot \vec{k}\, d\vec{X}. \qquad (71) \end{aligned}$$

The second term of (71), $\oint_{\partial\Omega}(1-k^2)\vec{k} \cdot \hat{n} ds$, goes to zero as $\epsilon \to 0$.

Applied to (69), (70) and (71) respectively imply

Proposition 5.1.

$$\mathcal{E}^\epsilon(\Theta^\epsilon) \leq -2\int_\Omega (\nabla \cdot \vec{k}^\epsilon_{SD})(1-(k^\epsilon_{SD})^2)\, d\vec{X}, \tag{72}$$

$$\mathcal{E}^\epsilon(\Theta^\epsilon) \leq -4\int_\Omega \vec{k}^\epsilon_{SD} \cdot \nabla\vec{k}^\epsilon_{SD} \cdot \vec{k}^\epsilon_{SD}\, d\vec{X} + \mathcal{O}(\epsilon). \tag{73}$$

In this evaluation the first term of (70) (resp. (71)) vanishes because the integrand of this term is precisely the self-dual operator.

In Section 4 we saw that the defect locus of a self-dual solution generically consisted of grain boundaries that could terminate at points or meet other grain boundaries at a point with three branches. In other words the defect locus Γ is a set that almost everywhere is a local one-dimensional manifold. The generic exceptions are terminal points where it has the form of a 1D manifold with boundary and spines where it has the form of the neighborhood of a graph vertex of valence 3.

We will express the bound (73) directly in terms of the jump in $\vec{k}$ along the defect. Set $\Theta^0 = d(\vec{X}) = \lim_{\epsilon\to 0}\Theta^{\epsilon}_{SD}$. The following lemma summarizes the asymptotic results from Section 4 that we will need.

Lemma 5.2.

1. *Outside of an arbitrarily small neighborhood of* Γ, $\vec{k}^0 = \nabla\Theta^0$ *satisfies* $|\vec{k}^0|^2 = 1$ *and* $\nabla\vec{k}^0 \cdot \vec{k}^0 = 0$.
2. *In coordinates adapted to a tubular neighborhood of* Γ, $\vec{k}^0_{tang}(\vec{X})$ *extends to a continuous function.* $\vec{k}^0_{norm}(\vec{X})$ *is discontinuous along* Γ *but bounded throughout* Ω. *The partial derivatives of* $\vec{k}^0_{tang}(\vec{X})$ *are uniformly bounded throughout* Ω.

Remark. Part 1 implies that up to contributions of order ϵ, it suffices to consider the integrand of (73) in an $\mathcal{O}(\epsilon)$ neighborhood of Γ. Part 2 follows from the jump conditions (64). Strictly speaking, the jump conditions do not apply at terminal points and spines. However, these are isolated points and in our application to the inequality (73) the value at these points will not affect the value of the integral.

Let $\vec{X}(\gamma)$ be a parametrization of a smooth branch of Γ and let ν be the coordinate along the normal direction in the tangent bundle to Γ. In a sufficiently narrow tubular neighborhood of Γ, $\vec{W} = (\gamma, \nu)$ is a smooth coordinate system. The change of coordinates is given by

$$\vec{X} = \vec{X}(\gamma) + \nu\hat{N}(\gamma),$$

where $\hat{N}(\gamma)$ is the unit normal along Γ. The unit tangent vector to Γ is $\hat{T}(\gamma) = \frac{\vec{X}'(\gamma)}{\sigma}$ where $\sigma = |\vec{X}'(\gamma)|$, the arclength parameter. We choose orientations of our parametrizations so that $\hat{N}$ is equal to $\hat{T}^{\perp}$. If $M = \frac{d\vec{W}}{d\vec{X}}$, the jacobian of the coordinate transformation, then the inverse is given by

$$M^{-1} = (\sigma\hat{T} + \nu\kappa\hat{T}, \hat{N}),$$

where we have used the Frenet formula $d/ds\ \hat{N} = -\kappa\hat{T}$ and $\kappa(\gamma)$ is the curvature of Γ. From this it is straightforward to calculate that the determinant $|M^{-1}| = \sigma + \nu\kappa$ and that

$$M = \frac{1}{\sigma + \nu\kappa}\begin{pmatrix} N_2 & -N_1 \\ -(\sigma + \nu\kappa)T_2 & (\sigma + \nu\kappa)T_1 \end{pmatrix}.$$

Here the components of $\hat{T}$ and $\hat{N}$ are with respect to $\vec{X}$ coordinates. If $\vec{K}$ is the gradient of Θ with respect to $\vec{W}$, then

$$\vec{k} = \vec{K}M$$

and

$$\nabla_{\vec{X}}\vec{k} = M^t \nabla_{\vec{W}}\vec{K}M.$$

Finally, if Γ does not branch, the integral (73) can be rewritten as

$$\int_{\Omega} \vec{k}\cdot\nabla\vec{k}\cdot\vec{k}^t\, d\vec{X} = \int_{\vec{W}^{-1}(\Omega)} \vec{K}MM^t\nabla_{\vec{W}}\vec{K}MM^t\vec{K}^t \quad |M^{-1}|\, d\vec{W}, \tag{74}$$

where the determinant $|M^{-1}| = \sigma + \nu\kappa$.

Theorem 5.3. *For Γ a smooth curve with boundary points,*

$$\mathcal{E}^{\epsilon}(\Theta^{\epsilon}) \leq -1/3 \int_{\Gamma} \left[\Theta^0_{\nu}\right]^3 d\sigma + \mathcal{O}(\epsilon).$$

With $\vec{K}^{\epsilon}_{SD} = (F^{\epsilon}, G^{\epsilon})$ and with $\alpha = \sigma + \nu\kappa$, one expands the estimate (73) as follows:

$$\begin{aligned}
\mathcal{E}^{\epsilon}(\Theta^{\epsilon}) &\leq -4\int_{\Gamma}\int_{-\epsilon}^{\epsilon} \alpha^{-4}F^{\epsilon}_{\gamma}(F^{\epsilon})^2 + 2\alpha^{-2}F^{\epsilon}_{\nu}F^{\epsilon}G^{\epsilon} + G^{\epsilon}_{\nu}(G^{\epsilon})^2\alpha\, d\nu d\gamma + \mathcal{O}(\epsilon)\\
&= -4\int_{\Gamma}\int_{-\epsilon}^{\epsilon} G^{\epsilon}_{\nu}(G^{\epsilon})^2\alpha\, d\nu\, d\gamma + \mathcal{O}(\epsilon)\\
&= -4\int_{\Gamma}\int_{-\epsilon}^{\epsilon} \Theta^{\epsilon}_{\nu}\Theta^{\epsilon}_{\nu\nu}\Theta^{\epsilon}_{\nu}\alpha\, d\nu\, d\gamma + \mathcal{O}(\epsilon)\\
&= -4/3\int_{\Gamma} \left(\Theta^{\epsilon}_{\nu}\right)^3 \Big|^{\epsilon}_{-\epsilon}\sigma\, d\gamma + \mathcal{O}(\epsilon)\\
&= -4/3\int_{\Gamma} \left(\Theta^{0}_{\nu}\right)^3 \Big|^{\epsilon}_{-\epsilon} d\sigma + \mathcal{O}(\epsilon)\\
&= -1/3\int_{\Gamma} \left[\Theta^0_{\nu}\right]^3 d\sigma + \mathcal{O}(\epsilon),
\end{aligned}$$

where $[\Theta^0_{\nu}]$ is the jump of this derivative across Γ. The inequality on the first line is just (73) rewritten in the tubular neighborhood coordinates $\vec{W}$. Up to terms of order ϵ we can restrict the integral to this tubular neighborhood by Lemma 5.2.1. Using the orthonormality of T, N, one sees that the product MM^t is the diagonal matrix

$$\begin{pmatrix} \alpha^{-2} & 0 \\ 0 & 1 \end{pmatrix}.$$

The second line is a consequence of Lemma 5.2.2 since the first two terms on the first line are uniformly bounded in a region of size ϵ. The next equality simply replaces G^{ϵ} by Θ^{ϵ}_{ν}, and we observe that this term is a perfect derivative which yields the equality on

the fourth line. The fifth line is then an immediate consequence of (60). Next observe that

$$\left[\Theta_\nu^0\right]^3 = \left(\Theta_\nu^0\big|_{-\epsilon}^{\epsilon}\right)^3 = (\Theta_\nu^0)^3(\gamma,\epsilon) - 3(\Theta_\nu^0)^2(\gamma,\epsilon)\Theta_\nu^0(\gamma,-\epsilon) + 3\Theta_\nu^0(\gamma,\epsilon)(\Theta_\nu^0)^2(\gamma,-\epsilon) - (\Theta_\nu^0)^3(\gamma,-\epsilon).$$

From (60) and Proposition 4.3 it follows that as $\epsilon \to 0$, $(\Theta_\nu^0)^2(\gamma,-\epsilon) = (\Theta_\nu^0)^2(\gamma,\epsilon) + \mathcal{O}(\epsilon)$ so that the RHS of the above equality becomes $4(\Theta_\nu^0)^3|_{-\epsilon}^{\epsilon}$, modulo terms of order ϵ. This gives the RHS of the inequality in Theorem (5.3).

Corollary 5.4. *Let Γ_i, $i = 1,\ldots,N$ be the smooth branches of a generic defect locus Γ. Then*

$$\mathcal{E}^\epsilon(\Theta^\epsilon) \le -1/3 \sum_{i=1}^{N} \int_{\Gamma_i} \left[\Theta_{\nu_i}^0\right]^3 d\sigma + \mathcal{O}(\epsilon),$$

where ν_i is the coordinate normal to Γ_i.

At a spine there are three rays from the disclination to the boundary of equal (minimal) distance. Cutting Ω along all such rays dissects it into N regions, each containing one of the branches Γ_i. The integral on the RHS of (73) equals the sum of such integrals over each region in the dissection. Applying Theorem (5.3) gives the corollary.

Corollary 5.5. *There is a constant C, independent of ϵ, such that for domains Ω with generic defect locus Γ,*

$$\int_\Omega |\nabla \vec{k}^\epsilon|^2 d\vec{X} \le C/\epsilon, \tag{75}$$

$$\int_\Omega (1-(k^\epsilon)^2)^2 d\vec{X} \le C\epsilon, \tag{76}$$

where $k^\epsilon = |\nabla\Theta^\epsilon|$. From (76) we may conclude that $|\nabla\Theta^\epsilon|^2 \to 1$ in $L^2(\Omega)$. It follows that there is a subsequence $\Theta^{\epsilon_j} \rightharpoonup \bar{\Theta}$ in $H^1(\Omega)$. This sequence converges strongly to $\bar{\Theta}$ in $L^2(\Omega)$.

The size of the jump $[\Theta_{\nu_i}^0]$ is bounded along Γ_i, which has finite length. Thus the sum over branches on the RHS of Corollary(5.4) is finite and therefore, for ϵ sufficiently small, $\mathcal{E}^\epsilon(\Theta^\epsilon)$ is less than a constant that is independent of ϵ. Since the energy (68) is the sum of two positive terms, this gives a uniform bound on each term; i.e., the bounds (75) and (76) hold. The rest of the corollary is a standard consequence of uniform boundedness.

We next turn to an estimation of a lower bound for $\mathcal{E}^\epsilon(\Theta^\epsilon)$. In this we follow an approach used by Jin and Kohn [28] in the context of thin film blisters. This approach has been successfully implemented to give a sharp lower bound only when the defect locus Γ is a straight line segment. In what follows we will restrict to this case. We shall take the straight segment to be parallel to the X-axis. For simplicity we also take $\alpha(s) = 0$ so that on the boundary, $\vec{k}$ is normal to $\partial\Omega$ and pointing inside Ω.

The idea of [28] is to seek a vector function of $\vec{k}$, call it $\vec{S}(\vec{k})$, such that

$$\int_\Omega \nabla \cdot \vec{S}(\vec{k})\, d\vec{X} \le \mathcal{E}^\epsilon(\vec{k})$$

for all $\vec{k}$. The term on the left will in fact be independent of $\vec{k} \in \mathcal{A}^\epsilon$ since by the divergence theorem it is equal to a boundary integral. As a guide to choosing $\vec{S}$ one observes that

$$\nabla \cdot \vec{S}(\vec{k}) = S_{1f}\Theta_{XX} + (S_{1g} + S_{2f})\Theta_{XY} + S_{2g}\Theta_{YY}.$$

One then tries to find an $\vec{S}$ whose partial derivatives can be related to the integrand of $\mathcal{E}^\epsilon$. The following choice,

$$\begin{aligned} \vec{S}(\vec{k}) &= 2\left(\int (1-k^2)\, df,\ -\int (1-k^2)\, dg\right) \\ &= 2\left(-1/3\, f^3 - fg^2 + f,\ 1/3g^3 + gf^2 - g\right), \end{aligned} \tag{77}$$

has partial derivatives proportional to $(1-k^2)$: $S_{1f} = 2(1-k^2)$, $(S_{1g} + S_{2f}) = 0$, $S_{2g} = -2(1-k^2)$. Using this one has the following estimate for the integrand:

$$\begin{aligned} \nabla \cdot \vec{S}(\vec{k}) &= 2(1-k^2)(\Theta_{XX} - \Theta_{YY}) \\ &\le \epsilon(\Theta_{XX} - \Theta_{YY})^2 + \epsilon^{-1}(1-k^2)^2 \\ &= \epsilon(\Theta_{XX} + \Theta_{YY})^2 + \epsilon^{-1}(1-k^2)^2 - 4\epsilon(\Theta_{XX}\Theta_{YY}) \\ &\le \epsilon(\nabla \cdot \vec{k})^2 + \epsilon^{-1}(1-k^2)^2 - 4\epsilon(\Theta_{XX}\Theta_{YY} - \Theta_{XY}^2). \end{aligned} \tag{78}$$

Modulo the last term, this gives the desired inequality. However, this term, which is proportional to the Hessian $[\Theta, \Theta]$ and equal to J, is a perfect divergence $2J = \nabla \cdot (fg_Y - gf_Y, gf_X - fg_X)$. Since for our problem $\vec{k}$ approaches magnitude 1 as $\epsilon \to 0$ everywhere on the boundary, we have, from (41) that

$$\int_\Omega 2[\Theta, \Theta]\, d\vec{X} = \oint_{\partial\Omega} k^2(s)\, d\phi(s) \ \to\ \text{winding number of } \vec{k} \text{ around } \partial\Omega;$$

i.e., it is asymptotically a purely topological invariant of the boundary data and therefore the last term, when integrated over Ω, is $\mathcal{O}(\epsilon)$.

We can now prove the equality of the upper and lower bounds in these cases.

Theorem 5.6. *If Γ is a straight horizontal line segment, then any L^2-convergent subsequence of the minimizing sequence Θ^ϵ for $\mathcal{E}^\epsilon$ on $\mathcal{A}^\epsilon$ converges to the self-dual limit Θ^0 in energy, i.e.,*

$$\mathcal{E}^\epsilon\left(\Theta^\epsilon\right) - \mathcal{E}^\epsilon\left(\Theta^\epsilon_{SD}\right) \to 0,$$

where in this formula we assume that ϵ indexes the convergent subsequence. Moreover, this limit is independent of the initial choice of a sequence of minimizers.

From (78) and (70) we respectively have

$$\begin{aligned} \text{Lower Bound} &= 2\int_\Omega \left(1 - (k^\epsilon_{SD})^2\right)\left((\Theta^\epsilon_{SD})_{XX} - (\Theta^\epsilon_{SD})_{YY}\right) d\vec{X} + \mathcal{O}(\epsilon), \\ \text{Upper Bound} &= -2\int_\Omega \left(1 - (k^\epsilon_{SD})^2\right)\left((\Theta^\epsilon_{SD})_{XX} + (\Theta^\epsilon_{SD})_{YY}\right) d\vec{X} + \mathcal{O}(\epsilon). \end{aligned} \tag{79}$$

The expression of the lower bound in (79) follows from the fact that the lower bound in (78) can be evaluated on any element of $\mathcal{A}^\epsilon$ since it really depends on only the boundary values of this element; in particular one can evaluate it on the self-dual solution. It follows from Lemma 5.2.2 that $\left(1-(k^\epsilon_{SD})^2)\right)(\Theta^\epsilon_{SD})_{XX} \to 0$ as $\epsilon \to 0$. Hence, the two bounds become asymptotically equal in this limit.

Although the proof of the above theorem uses the *bulk* representations of the upper and lower bounds, what is interesting and useful about these two bounds is that they are both also expressible as contour integrals. We illustrate this in two particular examples. The first example will be typical of the admissible class of (anti–)self-dual solutions whose asymptotics were studied in the previous section. The other, strictly speaking, falls outside this class but represents an extension for which the arguments given here generalize. In all these examples the defect locus Γ is a straight line segment.

In the first example, Ω is a domain whose boundary is an ellipse, with major axis along the X-axis. The defect locus Γ is the horizontal segment on the X-axis whose two endpoints are located at the two curvature centers of the ellipse and $\vec{k}|_{\partial\Omega}$ is proportional to $\hat{n}$. This choice of $\vec{k}$ on the boundary is justified a posteriori by checking the asymptotic behavior of the self-dual solution. It is straightforward to check that $\vec{S}(\vec{k})\cdot\hat{n} = -4/3(f^2 - g^2)$. Combining this lower estimate with (5.3) gives

$$-4/3\oint_{\partial\Omega}(\Theta_X^2-\Theta_Y^2)ds + \mathcal{O}(\epsilon) \le \mathcal{E}^\epsilon(\vec{k}^\epsilon) \le -1/3\int_\Gamma \left[\Theta_y^0\right]^3\, dX + \mathcal{O}(\epsilon). \qquad (80)$$

Using the parameterization

$$\vec{X} = (a\cos(t), b\sin(t)) \qquad (a > b),$$

the asymptotic lower and upper bounds can be respectively represented as

$$-4/3\oint_{\partial\Omega}(\Theta_X^2-\Theta_Y^2)ds \;=\; 4/3\int_0^{2\pi}\frac{b^2\cos^2(t)-a^2\sin^2(t)}{\sqrt{b^2\cos^2(t)+a^2\sin^2(t)}}\,dt,$$

$$-1/3\int_\Gamma\left[\Theta_Y^0\right]^3 dX \;=\; 8/3\int_{\frac{-(a^2-b^2)}{a}}^{\frac{a^2-b^2}{a}}\left(\frac{1-\frac{a^2X^2}{(a^2-b^2)^2}}{1-\frac{X^2}{a^2-b^2}}\right)^{3/2} dX.$$

By Theorem 5.6 these two contour integrals are equal, giving a nontrivial identity between elliptic integrals. What is remarkable about this result is that whereas $[\Theta, \Theta]$ is zero away from Γ, it is not zero in the neighborhood of Γ, where all the free energy resides, unlike the case of the "knee" solution (48). Rather, the solutions in the neighborhood of Γ resemble a modulated knee where, in the $\epsilon \to 0$ limit, the angle between the phase contour and the line defect Γ changes along Γ. So even though the boundary layer solutions of eqs. (18) and (47) may not agree, in the limit $\epsilon \to 0$, their jumps $[\Theta_Y^0]$, as functions of X measured along Γ do.

A second example is the case of the stadium (see Figure 16), consisting of horizontal stripes with two semicircular ends. The constant phase contours retain this shape, and the line defect is the straight line joining the centers of curvature of the semicircles (that are convex disclinations). Note that in this case there are *infinitely* many points on $\partial\Omega$ (along the semicircles) that are equidistant from a given convex disclination. This does not fall

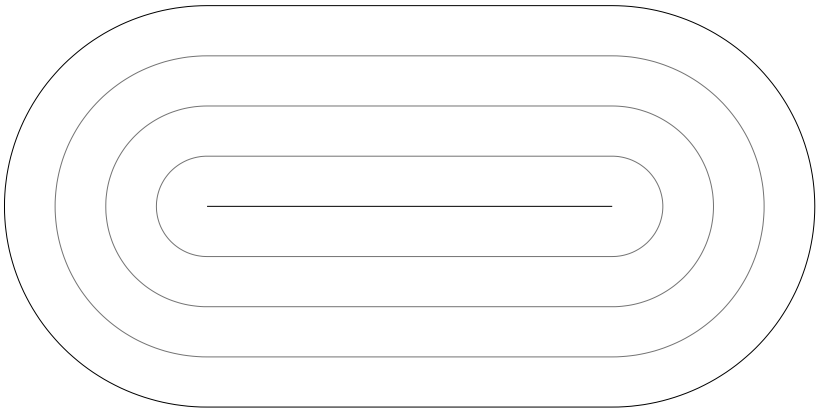

Fig. 16. "Stadium" comprised of two convex disclinations connected by a phase grain boundary.

within the class of defect asymptotics that we examined in the last section. Nevertheless one finds

$$\begin{aligned}\text{Lower Bound} &= -4/3 \int_\Gamma 2(f^2 - g^2)\, dX \\ &= -8/3 \int_\Gamma -dX = \frac{8}{3}\ell(\Gamma), \\ \text{Upper Bound} &= -1/3(-2)^3 \int_\Gamma dX = \frac{8}{3}\ell(\Gamma),\end{aligned}$$

where $\ell(\Gamma)$ is the length of Γ. In the upper bound the jump is constant, equal to -2, all along Γ. In the lower bound we use again the boundary evaluation $\vec{S}(\vec{k}) \cdot \hat{n} = -4/3(f^2 - g^2)$. There is a dominant equal contribution from each of the two straight sides parallel to Γ; there is no dominant contribution from the circular parts of the boundary. The integral over these portions $\mathcal{O}(\epsilon \log \epsilon)$. While this is stronger than the endpoint contribution for the ellipse, which is $\mathcal{O}(\epsilon)$, it nevertheless vanishes in the limit.

One of the principal motivations for the introduction of the RCN equation was to use it as a mechanism for selecting single-valued branches of multivalued CN solutions by taking the limit of RCN solutions as $\epsilon \to 0$. It is now natural to ask about the relation between the generic singularities of the hodograph solutions and the generic defects of Θ^0. In the free energy (39) we took $G^2 = (k^2 - 1)^2$. However, this was only for convenience. The results presented here hold for a much more general class of Ginzburg-Landau free energies [38]. The generalization of Corollary 5.5 to asymptotic minimizers of (44) suggests that these singular limits are special solutions of the CN equation that take values in the circle $k^2 = 1$. Such solutions have the hodograph jacobian, J, equal to 0 everywhere and correspond to so-called *simple* solutions of the quasilinear system (6) [30].

An important consequence of our analysis of self-dual solutions was Corollary 5.5, which shows that a subsequence of minimizers Θ^ϵ has a weak limit $\bar{\Theta}$ in $H^1(\Omega)$. It

is natural to think that one can pass to the limit in the relation $|\nabla\Theta^\epsilon| \to 1$ giving $|\nabla\bar{\Theta}| = 1$ almost everywhere. We further expect that $\bar{\Theta}$ has the form of a smooth solution of the eikonal equation, $|\nabla\bar{\Theta}| = 1$, except along jump discontinuities and that the set of jump discontinuities is a countable union of rectifiable curves; indeed, as we have shown, the asymptotic limit of the self-dual solutions has precisely this form. However, even if one knew that, asymptotically, the energy $\mathcal{E}^\epsilon(\Theta^\epsilon)$ tends to the energy of the asymptotic self-dual solution (as we do in the case of Theorem 5.6), one could not conclude that the asymptotic minimizer has this form since it may be that $\{\Theta^\epsilon\}$ and $\{\Theta^\epsilon_{SD}\}$ have the same asymptotic energy without limiting to the same element of $H^1(\Omega)$.

Nevertheless, assume that in addition to what we have already proved about $\bar{\Theta}$ one knew that the components $\bar{f}, \bar{g}$ of $\nabla\bar{\Theta}$ were of bounded variation (BV). In this case there is a decomposition theorem [2], [6] for $Hess(\bar{\Theta})$, regarded as a measure, which states that the jump discontinuities of $\nabla\bar{\Theta}$ are supported on a set, Σ, of one-dimensional Hausdorff measure. Then, at least, the defect set Σ for $\bar{\Theta}$ would consist of a countable union of rectifiable curves, and one expects that the asymptotic energy will concentrate on Σ with strength given as a function of the jump in $\vec{k}$ across Σ. It has been conjectured by Ortiz and Gioia [50] and Aviles and Giga [5], based on scaling arguments, that the asymptotic minimum of $\mathcal{E}^\epsilon(\Theta)$ is realized as

$$J(\bar{\Theta}) = \frac{1}{3}\int_\Sigma |[\nabla\bar{\Theta}]|^3\, d\sigma. \tag{81}$$

Aviles and Giga [5] have shown that if, in addition to the other assumptions, one also assumes that $\nabla\Theta^\epsilon$ converges to $\nabla\bar{\Theta}$ in $L^3(\Omega)$, then $J(\bar{\Theta}) \le \liminf_{\epsilon\to 0}\mathcal{E}^\epsilon(\Theta^\epsilon)$.

Although in many cases it can be demonstrated that the distance function, Θ^0, realizes the minimum of $J(\Theta)$ over H^1 functions with BV gradient and satisfying the eikonal equation with the asymptotic boundary conditions, there are counterexamples for non-convex domains Ω [28], [6] which show that it does not have to be unique. This raises the possibility that although Θ^ϵ may converge to Θ^0 in energy, it may not converge to it in any stronger sense. It should however be pointed out that for the counterexamples cited above, the boundary $\partial\Omega$ was not smooth.

Finally we discuss how to realize patterns with twist $= \pm 1$ as singular limits of the regularized phase diffusion equation. To achieve this in general one would need to consider spaces consisting of double-valued functions, the double-valuedness corresponding to the orientational ambiguity of director fields. One way to do this concretely would be to consider single-valued functions on domains which are two-sheeted Riemann surfaces rather than simply connected planar domains. However, in the variational setting of Section 5 one would then need to consider variations over Riemann surfaces as well as functions. This would be an ambitious undertaking, and so for the present we have restricted our considerations to examples in which there is some symmetry that isolates the structure of the Riemann surface. We will illustrate this for the case of the concave disclination. Figure 7 shows a numerical solution of the stationary RCN equation that has the form of a concave disclination. The Riemann surface used in this simulation was the double cover $\tilde{\Omega}$ of a disc, Ω, given by the covering map

$$\mathcal{F}\colon\ \vec{W} = (U, V) \mapsto \vec{X} = (X, Y) = (U^2 - V^2, 2UV). \tag{82}$$

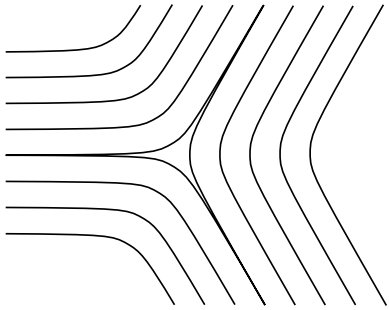

Fig. 17. Three knees.

The pullback of the energy $\mathcal{E}^\epsilon(\Theta)$ to $\tilde{\Omega}$ will depend explicitly on r in that

$$\int_\Omega (\Delta\Theta)^2 \, d\vec{X}$$

gets replaced by

$$\int_{\tilde{\Omega}} \frac{(\tilde{\Delta}\Theta)^2}{4(U^2+V^2)} \, d\vec{W},$$

where $\tilde{\Delta}$ is the Laplacian on $\tilde{\Omega}$. The solutions shown in Figures 7 and 8 were found by numerically solving the variational equations of the pulled back energy on $\tilde{\Omega}$ with boundary conditions given by pulling back the double-valued boundary data of the hodograph solutions of the CN equation on $\partial\Omega$ to single-valued boundary values on $\partial\tilde{\Omega}$.

To study this concave disclination analytically we want to use self-dual solutions again. Because of the explicit r-dependence of the pulled back energy density, one doesn't have a direct reduction of the self-dual equation to a Helmholtz equation. However, for the particular case we are considering one can build appropriate test functions directly by patching together the knee solutions (48) of the Helmholtz equation. Specifically we use a form of the knee with a parameter α that exhibits roll-bending through an angle of $\pi - 2\alpha$:

$$\Theta^\epsilon_\alpha = -\epsilon \log \psi = \cos(\alpha)x - \epsilon \log\cosh(\sin(\alpha)y/\epsilon). \tag{83}$$

An approximation to a regularized concave disclination is realized by patching together three copies of (83) with $\alpha = \pi/6$. The two other sectors are constructed by rotating Θ^ϵ_α through $2\pi/3$, $-2\pi/3$ radians, respectively. The pairwise common boundaries of these three 120° sectors are the rays $\alpha = -\pi/3$, $\alpha = \pi$, and $\alpha = \pi/3$ (see Figure 17). The patching across these rays is not smooth; there is a jump in the direction of $\vec{k}$ as one crosses each ray (there is no jump in the magnitudes). However, as $\epsilon \to 0$, the jump in the direction of $\vec{k}$ is either 0 or π (this ambiguity is due to the ambiguity of the twist). Proceeding counterclockwise, if one consecutively chooses the matching so that this jump is 0 (i.e., there is no jump) then, after making a full circuit from the ray $\alpha = \pi/3$ back to itself, $\vec{k}$ will return with the opposite orientation. If one makes two circuits it will return to itself. It is natural therefore to think of this as a two-valued solution. For $\epsilon > 0$

there is a jump in $\vec{k}$ across the rays even if we view the solution as two-valued. However, these jumps can be smoothed with bump functions so that in the limit as $\epsilon \to 0$ one gets the same result as in the unsmoothed case. The pullback of $\Theta^{\epsilon}_{\alpha}$ under $\mathcal{F}$ consists of two branches: $\Theta^{\epsilon,-}_{\alpha}$ is the branch with $0 < \nu < \pi$ and $\Theta^{\epsilon,+}_{\alpha}$ is the branch with $\pi < \nu < 2\pi$. Similarly, set $\Theta^{\epsilon,\pm}_{\alpha,\beta}$ equal to the corresponding branch of the pullback of $\Theta^{\epsilon}_{\alpha}$ rotated through β radians. Let $\phi^{\epsilon,\pm}_{\beta}$ be a bump function satisfying $\phi^{\epsilon,\pm}_{\beta} = 1$ if $\Theta^{\epsilon,\pm}_{\alpha,\beta} > \epsilon/2$ and $\phi^{\epsilon,\pm}_{\beta} = 0$ if $\Theta^{\epsilon,\pm}_{\alpha,\beta} < -\epsilon/2$. Then the patched three-knee solution on the double cover is given by

$$\begin{aligned}\chi^{\epsilon} \;=\; & \phi^{\epsilon,-}_{0}\Theta^{\epsilon,-}_{\alpha,0} - \phi^{\epsilon,-}_{2\pi/3}\Theta^{\epsilon,-}_{\alpha,2\pi/3} + \phi^{\epsilon,-}_{-2\pi/3}\Theta^{\epsilon,-}_{\alpha,-2\pi/3} \\ & - \phi^{\epsilon,+}_{0}\Theta^{\epsilon,+}_{\alpha,0} + \phi^{\epsilon,+}_{2\pi/3}\Theta^{\epsilon,+}_{\alpha,2\pi/3} - \phi^{\epsilon,+}_{-2\pi/3}\Theta^{\epsilon,+}_{\alpha,-2\pi/3}.\end{aligned}$$

For all positive ϵ, this function is smooth on the double cover. The function class $\mathcal{A}^{\epsilon}$ will be taken to have double-valued Dirichlet data coinciding with that of the patched test function, χ^{ϵ}, constructed above. We then have the analogue of the minimization inequality (69):

$$\mathcal{E}^{\epsilon}(\Theta^{\epsilon}) \le \mathcal{E}^{\epsilon}(\chi^{\epsilon}). \tag{84}$$

From (83) one calculates

$$\begin{aligned}1 - k(\chi^{\epsilon})^2 \;&=\; \mathcal{O}(\sin^2(\alpha)\operatorname{sech}^2(\sin(\alpha)y/\epsilon)), \\ |\nabla\vec{k}(\chi^{\epsilon})| \;&=\; \mathcal{O}((\sin^2(\alpha)/\epsilon)\operatorname{sech}^2(\sin(\alpha)y/\epsilon)).\end{aligned}$$

The leading order growth of $|\nabla\vec{k}(\chi^{\epsilon})|$ comes entirely from the defects forming along the rays $\alpha = 0, \alpha = 2\pi/3, \alpha = -2\pi/3$. There is no contribution to the blowup coming from the smoothed interfaces where the patching is done. From these last estimates one can deduce the fundamental estimates of Corollary 5.5 as before.

The covering (82) used to "untwist" the data of the concave disclination was a double cover of the disc branched at the origin. One might ask if there aren't double covers of the disc, possibly branched at more than one point, which would produce other double-valued solutions having lower energy than that of the three-knees and leading to a different limit as $\epsilon \to 0$. For topological reasons there can be only one branch point. The Hurwitz formula for the Euler characteristic $E(\tilde{\Omega})$ is

$$E(\tilde{\Omega}) = 2E(\Omega) - b,$$

which gives the relation between the Euler characteristic of the base disc Ω and the cover $\tilde{\Omega}$. Here b is the number of branch points. Since the Euler characteristic of a disc $= 1$, we find $b = 1$.

Since the data for the concave disclination is symmetric with respect to rotation by 120°, the branch point must be located at the origin.

6. Conclusion

In this paper we have analytically constructed multivalued solutions of the CN equation using the hodograph method. This method does a remarkably good job of qualitatively

reproducing isolated defects of patterns seen in experiments and simulations far from threshold. In the microscopic vicinity of the defects these solutions are multivalued and therefore not physical. We view this as a success rather than a failure of the theory, since the modulational ansatz of slow variation of the wavevector, under which the CN equation is derived, is certainly violated in the vicinity of a defect. Thus the formation of caustics in the CN equation identifies locations where the microscopic equations exhibit rapid variations of $\vec{k}$. The Legendre transform that underlies the hodograph method is quite interesting in that the dual variables which it relates, $\vec{X}$ and $\vec{k}$, are also the dual variables of the Fourier transform. Thus one can think of the solution of the linear hodograph equation (21) as the distribution of wavevectors over physical space. Reference [10] discusses a wavelet algorithm for finding this distribution in experimental and numerical patterns.

In order to compensate for the breakdown of the modulational ansatz and the concurrent appearance of multivaluedness in solutions of the CN equation, we introduced a fourth-order regularization of CN. We have shown that the RCN equation exhibits patterns and defects qualitatively similar to those of the original microscopic equations.

A fundamental contribution of this paper to the analysis of asymptotic minimizers of the RCN free energy is contained in Theorem 5.3 and Corollaries 5.4 and 5.5, which are based on the use of (anti–)self-dual solutions as test functions and the extension of these results to some examples having total twist ± 1. These provide the basis for the existence of asymptotic minimizers of the free energy (39) that solve the eikonal equation, $|\nabla\Theta| = 1$ almost everywhere, and give effective upper bounds for the asymptotic energy of the minimizers.

When the Dirichlet boundary conditions for the fourth-order RCN equation are chosen to be consistent with the solutions of the second-order self-dual equation, the self-dual solutions can realize tight upper bounds for the asymptotic energy. This was demonstrated when the defect of the self-dual solution is a straight line segment. This same result was found by Jin and Kohn [28] who were motivated by the problem of blistering of thin films. However, for calculating the upper bound they use test functions corresponding to nearly one-dimensional solutions rather than (anti–)self-dual solutions. The latter have the advantage that they can be used for any domain, including nonconvex domains, as long as the boundary is smooth and the Dirichlet boundary conditions for RCN are consistent with being solutions of a second-order (anti–)self-dual equation. On the other hand, the test functions used in [28] don't have these latter constraints. The example of the stadium shows that tight bounds on the asymptotic energy can also be realized by self-dual solutions when there are point defects with odd twist. A natural question concerns the classification of defects of the self-dual solutions in three dimensions. We have begun to consider this question and it is interesting to note [57], [22] that the self-dual solutions are solutions to the higher dimensional RCN equation away from places where the sectional curvatures of the surface are nonvanishing.

We have constructed explicit solutions of the hodograph equation in Section 3 that illustrate the generic singularities of such solutions. We have also described the generic defects of Θ^0 in Theorem 4.4. Point defects were defined in the context of multivalued solutions of the CN equation. There are still many unanswered questions. What are the analogues of the point defects in the context of asymptotic minimizers? We

have already defined spines and terminal points in terms of defects of Θ^0, but what about the concave and convex disclinations? The asymptotic behavior of the Hessian, $[\Theta^\epsilon, \Theta^\epsilon]$, appears to provide a mechanism for distinguishing these disclinations. This Hessian is proportional to the Gaussian curvature of the surface corresponding to the graph of Θ. In the numerical simulations such as those shown in Figures 7 and 8, we have observed that $[\Theta^\epsilon, \Theta^\epsilon]$ tends to zero everywhere except in the vicinity of the point disclinations. On the other hand, in the case of the ellipse the nonzero asymptotic values of $[\Theta^\epsilon, \Theta^\epsilon]$ are distributed all along the grain boundary between the two terminal points. Thus we are led to provisionally define a disclination of an asymptotic minimizer to be a point at which the Hessian of the sequence $\{\Theta^\epsilon\}$ concentrates.

Although admittedly based on a small amount of evidence, the following seems to us to be a natural conjecture for the form of the ϵ expansion of the energy in terms of defects:

$$\mathcal{E}^\epsilon(\Theta^\epsilon) = J(\bar{\Theta}) + \epsilon \log(\epsilon) T(\bar{\Theta}) + \mathcal{O}(\epsilon),$$

where $J(\bar{\Theta})$ is the jump energy (81) of the asymptotic minimizer and T depends on the configuration of point disclinations, as defined in the previous paragraph, in Ω of the twist of each disclination. The associated densities of J and T are natural measures in terms of which to give a reduced description of the structure and dynamics of defects in patterns. Although much remains to be done to establish this description, what we have shown in this paper supports it and provides the first steps toward proving it.

Acknowledgments

The authors would like to express their appreciation to J. Lega for helpful discussions and a critical reading of the manuscript. The authors would like to acknowledge the support received from NSF Grants DMS-9302013 and DMS-9626306, and AFOSR Grant F49620-94-1-0144. T. Passot gratefully acknowledges the hospitality of the Arizona Center for Mathematical Sciences.

References

[1] M. Abramowitz and I. Stegun. *Handbook of Mathematical Functions*. U.S. Govt. Printing Office, Washington, D.C., 1972.

[2] G. Alberti. Rank one property for derivatives of functions with bounded variation. *Proc. Roy. Soc. Edinburgh Sect. A*, 123:239–274, 1993.

[3] V. I. Arnold, S. M. Gusein-Zade, and A. N. Varchenko. *Singularities of Differentiable Mappings Volume 1*. Birkhäuser, Boston, 1985.

[4] M. Assenheimer and V. Steinberg. Rayleigh-Bénard convection near the gas-liquid critical point. *Phys. Rev. Lett.*, 70:3888–3891, 1993.

[5] P. Aviles and Y. Giga. On lower semicontinuity of a defect energy obtained by a singular limit of the Ginzburg-Landau type energy for gradient fields. *Proc. Roy. Soc. Edinburgh Sect. A*, in press.

[6] P. Aviles and Y. Giga. The distance function and defect energy. *Proc. Roy. Soc. Edinburgh Sect. A*, 126:923–938, 1996.
[7] F. Bethuel, H. Brezis, and F. Hélein. *Ginzburg-Landau Vortices*. Birkhäuser, Boston, 1994.
[8] E. Bodenschatz. Private communication, 1997.
[9] C. Bowman, N. Ercolani, R. Indik, A. C. Newell, and T. Passot. Patterns, defects and integrability. *Physica D*, 123:474–492, 1998.
[10] C. Bowman, T. Passot, M. Assenheimer, and A. C. Newell. A wavelet based algorithm for pattern analysis. *Physica D*, 119:250–282, 1998.
[11] F. H. Busse. Nonlinear properties of thermal convection. *Rep. Prog. Phys.*, 41:1929–1967, 1978.
[12] F. H. Busse and R. M. Clever. Mechanisms of the onset of time-dependent in thermal convection. *Time-Dependent Nonlinear Convection*, P.A. Tygvand, ed.:1–49, Computational Mechanics Publications, Boston, 1998.
[13] R. E. Caflisch, N. M. Ercolani, T. Y. Hou, and Y. Landis. Multi-valued solutions and branch point singularities for nonlinear hyperbolic or elliptic systems. *Commun. Pure Appl. Math.*, 46:453–499, 1993.
[14] G. F. Carrier and C. E. Pearson. *Partial Differential Equations: Theory and Technique*. Academic Press, New York, 1988.
[15] S. Chandrasekhar. *Hydrodynamic and hydromagnetic stability*. Clarendon Press, Oxford, 1961.
[16] P. Collet and J. P. Eckmann. *Instabilities and Fronts in Extended Systems*. Princeton University Press, Princeton, NJ, 1990.
[17] R. Courant and K. O. Friedrichs. *Supersonic Flow and Shock Waves*. Interscience Publishers, New York, 1948.
[18] M. C. Cross and P. C. Hohenberg. Pattern formation outside of equilibrium. *Rev. Mod. Phys.*, 65(3):851–1112, 1993.
[19] M. C. Cross and A. C. Newell. Convection patterns in large aspect ratio systems. *Physica D*, 10:299, 1984.
[20] J. G. Dubois and J. P. Dufour. Singularities de solutions d'équations aux dérivées partielles. *J. Diff. Eqns.*, 60:174–200, 1985.
[21] J. P. Eckmann, C. E. Wayne, and P. Wittwer. Geometric stability analysis of periodic solutions of the Swift-Hohenberg equation. *Commun. Math. Phys.*, 190:173–211, 1997.
[22] N. Ercolani, R. Indik, A. C. Newell, and T. Passot. Singularities, defects and twist in phase diffusion equations. In preparation.
[23] L. C. Evans. *Partial Differential Equations*. American Mathematical Society, Providence, RI, 1998.
[24] P. R. Garabedian. *Partial Differential Equations*. John Wiley, New York, 1964.
[25] H. Ishii and S. Koike. Remarks on elliptic singular perturbation problems. *Appl. Math. Optim.*, 23:1–15, 1991.
[26] A. Jaffe and C. Taubes. *Vortices and Monopoles*. Birkhäuser, Boston, 1980.
[27] P. K. Jakobsen, J. Lega, Q. Feng, M. Staley, J. V. Moloney, and A. C. Newell. Nonlinear transverse modes of large-aspect-ratio homogeneously broadened lasers: I. Analysis and numerical simulation. *Phys. Rev. A*, 49:4189, 1994.
[28] W. Jin and R. Kohn. Singular perturbation and the energy of folds. *J. Nonlin. Sci.*, 10, 2000, in press.
[29] A. Joets and R. Ribotta. Localized bifurcations and defect instabilities in the convection of a nematic liquid crystal. *J. Stat. Phys.*, 64:981–1005, 1991.
[30] F. John. *Partial Differential Equations*. Springer-Verlag, New York, 1986.
[31] M. Kleman. *Points, Lines, and Walls*. John Wiley, New York, 1983.
[32] R. Kohn and S. Muller. Relaxation and regularization of nonconvex variational problems. *Rend. Sem. Mat. Fis. Univ. Milano*, 62:89–113, 1992.
[33] N. Kopell and L. N. Howard. Slowly varying waves and shock structures in reaction-diffusion equations. *Stud. Appl. Math.*, 56:95–145, 1977.
[34] L. Kramer and W. Pesch. Convection instabilities in nematic liquid crystals. *Ann. Rev. Fluid Mech.*, 27:515–541, 1995.

[35] Y. Kuramoto. *Chemical Oscillations, Waves and Turbulence*. Springer-Verlag, New York, 1984.
[36] J. Lega, P. K. Jakobsen, J. V. Moloney, and A. C. Newell. Nonlinear transverse modes of large-aspect-ratio homogeneously broadened lasers: II. Pattern analysis near and beyond threshold. *Phys. Rev. A*, 49:4201, 1994.
[37] J. Lega, J. V. Moloney, and A. C. Newell. Swift-Hohenberg equation for lasers. *Phys. Rev. Lett.*, 73:2978, 1994.
[38] E. H. Lieb and M. Loss. Symmetry of the Ginzburg-Landau minimizer in a disc. *Math. Res. Lett.*, 1:701–715, 1994.
[39] F. H. Lin. Nonlinear theory of defects in nematic liquid crystals; phase transition and flow phenomena. *Commun. Pure Appl. Math.*, 42:789–914, 1989.
[40] P. L. Lions. *Generalized Solutions of Hamilton-Jacobi Equations*. Pitman Advanced Publishing Program, Boston, 1982.
[41] A. Lobkovsky, S. Gentges, H. Li, D. Morse, and T. A. Witten. Scaling properties of stretching ridges in a crumpled elastic sheet. *Science*, 270:1482–1485, 1995.
[42] P. Manneville and Y. Pomeau. Stability and fluctuations of a spatially periodic convection flow. *J. Phys. (Paris) Lett.*, 40:609–612, 1979.
[43] N. D. Mermin. The topological theory of defects in ordered media. *Rev. Mod. Phys.*, 51:591, 1979.
[44] A. C. Newell, T. Passot, C. Bowman, N. M. Ercolani, and R. Indik. Defects are weak and self-dual solutions of the Cross-Newell phase diffusion equation for natural patterns. *Physica D*, 97:185–205, 1996.
[45] A. C. Newell, T. Passot, and J. Lega. Order parameter equations for patterns. *Ann. Rev. Fluid Mech.*, 25:399–453, 1993.
[46] A. C. Newell, T. Passot, and M. Souli. The phase diffusion and mean drift equations for convection at finite Rayleigh numbers in large containers. *J. Fluid Mech.*, 220:187–252, 1990.
[47] A. C. Newell and J. A. Whitehead. Finite bandwidth, finite amplitude convection. *J. Fluid Mech.*, 38:279–303, 1969.
[48] J. C. Nitsche. *Lectures on Minimal Surfaces*. Cambridge University Press, New York, 1989.
[49] C. Normand, Y. Pomeau, and M. G. Verlarde. Convective instability: A physicist's approach. *Rev. Mod. Phys.*, 49:581, 1977.
[50] M. Ortiz and G. Gioia. The morphology and folding patterns of buckling driven thin film blisters. *J. Mech. Phy. Solids*, 42:531–559, 1994.
[51] T. Passot and A. C. Newell. Towards a universal theory of patterns. *Physica D*, 74:301–352, 1994.
[52] B. B. Plapp, D. A. Egolf, E. Bodenschatz, and W. Pesch. Dynamics and selection of giant spirals in Rayleigh-Bénard convection. *Phys. Rev. Lett.*, 81:5334–5337, 1998.
[53] B. Plapp. Spiral pattern formation in Rayleigh-Bénard convection. Dissertation, Cornell University, Ithaca, NY, 1997.
[54] Y. Pomeau. Caustics of nonlinear waves and related questions. *Europhys. Lett.*, 11:713–718, 1990.
[55] G. Schneider. Diffusive stability of spatial periodic solutions of the Swift-Hohenberg equation. *Commun. Math. Phys.*, 178, 1996.
[56] L. A. Segel. Distant side-walls cause slow amplitude modulation of cellular convection. *J. Fluid Mech.*, 38:203–224, 1969.
[57] B. Shipman. Private communication, 1995.
[58] H. Uecker. Diffusive stability of rolls in the two-dimensional real and complex Swift-Hohenberg equation. Preprint, 1998.
[59] G. B. Whitham. *Linear and Nonlinear Waves*. John Wiley and Sons, New York, 1974.
[60] H. Whitney. On singularities of mappings of Euclidean spaces: I. Mapping the plane into the plane. *Ann. Math.*, 62:374–410, 1955.